Chapter 7
System Design

In this chapter, we consider certain aspects of the design of the interferometric system in more detail. This discussion primarily involves parts of the system where the signals are in analog form. The trend in technology has been to convert signals as early as possible in the signal chain, following the antennas, into digital form to facilitate data handling, avoid low-level distortions, and generally take advantage of the rapid progress in the development of digital equipment and computers. Three key items are discussed: (1) low noise amplification of signals at the antenna output to minimize the effect of additive noise, (2) phase-stable transmission systems that allow the transfer of reference timing and phase signals from the central communications hub of the instrument to the antennas, and (3) the synchronous phase switching systems needed to eliminate spurious responses in the correlator output. The analysis here leads to specification of tolerances on system parameters that are necessary to achieve the goals of sensitivity and accuracy.

7.1 Principal Subsystems of the Receiving Electronics

Optimum techniques and components for implementation of the electronic hardware vary continuously as the state of the art advances, and descriptions in the literature provide examples of the practical techniques current at various times: see, for example, Read (1961), Elsmore et al. (1966), Baars et al. (1973), Bracewell et al. (1973), Wright et al. (1973), Welch et al. (1977, 1996), Thompson et al. (1980), Batty et al. (1982), Erickson et al. (1982), Napier et al. (1983), Sinclair et al. (1992), Young et al. (1992), Napier et al. (1994), de Vos et al. (2009), Perley et al. (2009), Wootten and Thompson (2009), and Prabu et al. (2015). The earlier papers in this list are mainly of interest from the viewpoint of the development of the technology.

A.R. Thompson, J.M. Moran, and G.W. Swenson Jr., *Interferometry and Synthesis in Radio Astronomy*, Astronomy and Astrophysics Library,
DOI 10.1007/978-3-319-44431-4_7

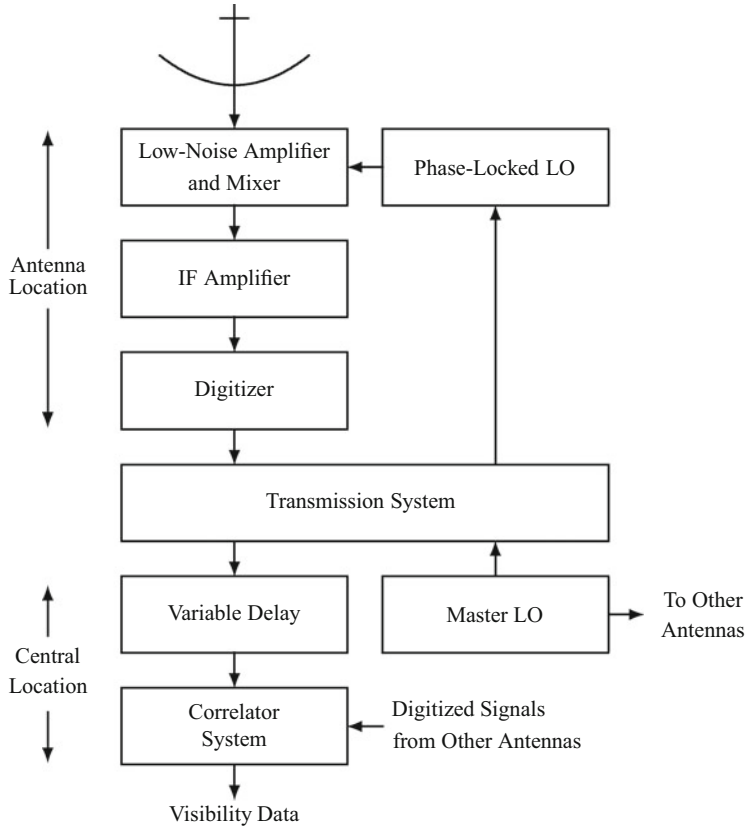

Fig. 7.1 Basic elements of the receiving system of a synthesis array. Here, the received signals are converted to an intermediate frequency (IF), digitized, and then transmitted by optical fiber to the central location for the derivation of visibility data. In systems of earlier design, and some smaller systems, the IF signal is transmitted to the central location in analog form and then digitized. LO indicates a local oscillator (i.e., usually one within the receiving system).

Figure 7.1 shows a simplified schematic diagram of the receiving system associated with one antenna of a synthesis array. Note that digitization of the signals is introduced as early as possible in the system, thus allowing most of the signal processing to be implemented digitally. In very early interferometers, there was no digitization, and the output was displayed on a chart recorder. In the original VLA system, the digitization occurred at the central location just before the delay and correlator processing. In the later VLA system (Perley et al. 2009), the signals are digitized at the antenna stations.

7.1.1 Low-Noise Input Stages

In radio astronomy receivers, minimizing the noise temperature usually involves cryogenic cooling of the amplifier or mixer stages from the input up to a point

at which noise from succeeding stages is unimportant. The low-noise input stages are often packaged with a cooling system, and sometimes also a feed horn, in a single package often referred to as the *front end*. The active components are usually transistor amplifiers or, for millimeter wavelengths, SIS (superconductor–insulator–superconductor) mixers followed by transistor amplifiers. For descriptions, see, for example, Reid et al. (1973), Weinreb et al. (1977a), Weinreb et al. (1982), Casse et al. (1982), Phillips and Woody (1982), Tiuri and Räisänen (1986), Payne (1989), Phillips (1994), Payne et al. (1994), Webber and Pospieszalski (2002), and Pospieszalski (2005).

In discussing the level of noise associated with a receiver, we begin by considering the case in which the Rayleigh–Jeans approximation suffices. This is the domain in which $h\nu/kT \ll 1$, where h is Planck's constant and T is the temperature of the thermal noise source involved. As noted in the discussion following Eq. (1.1), this condition can be written as ν (GHz) $\ll 20T$, where T is the system noise temperature in kelvins. It is convenient to specify noise power in terms of the temperature of a resistive load matched to the receiver input. In the Rayleigh–Jeans approximation, noise power available at the terminals of a resistor at temperature T is $kT\Delta\nu$, where k is Boltzmann's constant and $\Delta\nu$ is the bandwidth within which the noise is measured (Nyquist 1928). One kelvin of temperature represents a power spectral density of $(1/k)$ W Hz^{-1}. The receiver temperature T_R is a measure of the internally generated noise power within the system and is equal to the temperature of a matched resistor at the input of a hypothetical noise-free (but otherwise identical) receiver that would produce the same noise power at the output. The system temperature, T_S, is a measure of the total noise level and includes, in addition to T_R, the noise power from the antenna and any lossy components between the antenna and the receiver:

$$T_S = T'_A + (L-1)T_L + LT_R \ , \tag{7.1}$$

where T'_A is the antenna temperature resulting from the atmosphere and other unwanted sources of noise, L is the power loss factor of the transmission line from the antenna to the receiver [defined as (power in)/(power out)], and T_L is the temperature of the line. In defining the noise temperature of the receiver, we should note that in practice, a receiver is always used with the input attached to some source impedance that is itself a source of noise. The noise at the receiver output thus consists of two components, the noise from the source at the input, which is the antenna and transmission line in Eq. (7.1), and the noise generated within the receiver.

7.1.2 Noise Temperature Measurement

The noise temperature of a receiver is often measured by the Y-factor method. The thermal noise sources used in this measurement are usually impedance-matched

resistive loads connected to the receiver input by waveguide or coaxial line. The receiver input is connected sequentially to two loads at temperatures T_{hot} and T_{cold}. The measured ratio of the receiver output powers in these two conditions is the factor Y:

$$Y = \frac{T_R + T_{\text{hot}}}{T_R + T_{\text{cold}}} , \tag{7.2}$$

and thus,

$$T_R = \frac{T_{\text{hot}} - YT_{\text{cold}}}{Y - 1} . \tag{7.3}$$

Commonly used values are $T_{\text{hot}} = 290$ K (ambient temperature) and $T_{\text{cold}} \simeq 77$ K (liquid nitrogen temperature). For very precise measurements of T_R, it is important to note that the boiling point of liquid nitrogen depends on the ambient pressure.

The receiver temperature can be expressed in terms of the noise temperatures of successive stages through which the signal flows [see, e.g., Kraus (1986)]:

$$T_R = T_{R1} + T_{R2}G_1^{-1} + T_{R3}(G_1G_2)^{-1} + \cdots . \tag{7.4}$$

Here T_{Ri} is the noise temperature of the ith receiver stage, and G_i is its power gain. If the first stage is a mixer instead of an amplifier, G_1 may be less than unity, and the second-stage noise temperature then becomes very important.

For cryogenically cooled receivers for millimeter and shorter wavelengths, the Rayleigh–Jeans approximation can introduce significant errors. The power spectral density (power per unit bandwidth) of the noise is no longer linearly proportional to the temperature of the radiator or source. The ratio h/k is equal to 0.048 K per gigahertz, so if, for example, $T = 4$ K (liquid helium temperature), then $h\nu/kT = 1$ for $\nu = 83$ GHz. Thus, quantum effects become important as frequency is increased and temperature decreased. Under these conditions, the noise power per unit bandwidth divided by k provides an effective noise temperature that can be used in noise calculations, instead of the physical temperature. Two formulas are in use that give the effective temperature for a thermal source when quantum effects become important. One is the Planck formula and the other the Callen and Welton formula (Callen and Welton 1951). The effective noise temperatures for a waveguide carrying a single mode and terminated in a thermal load, or for a transmission line terminated in a resistive load, given by the two formulas are as follows:

$$T_{\text{Planck}} = T\left[\frac{\frac{h\nu}{kT}}{e^{h\nu/kT} - 1}\right] \tag{7.5}$$

$$T_{\text{C\&W}} = T\left[\frac{\frac{h\nu}{kT}}{e^{h\nu/kT} - 1}\right] + \frac{h\nu}{2k} , \tag{7.6}$$

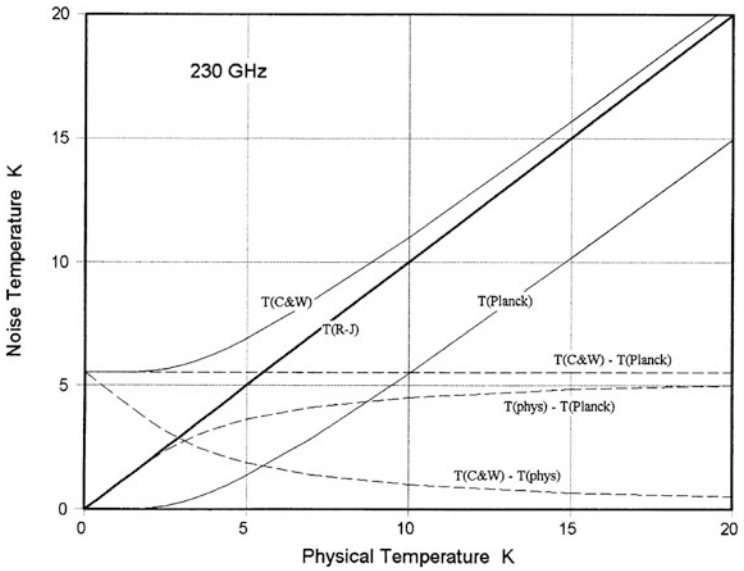

Fig. 7.2 Noise temperature vs. physical temperature for blackbody radiators at 230 GHz, according to the Rayleigh–Jeans, Planck, and Callen and Welton formulas. Also shown (broken lines) are the differences between the three radiation curves. The Rayleigh–Jeans curve converges with the Callen and Welton curve at high temperature, while the Planck curve is always $h\nu/2k$ below the Callen and Welton curve. From Kerr et al. (1997).

where T is the physical temperature. From Eqs. (7.5) and (7.6), we have

$$T_{\mathrm{C\&W}} = T_{\mathrm{Planck}} + \frac{h\nu}{2k} \,. \tag{7.7}$$

The Callen and Welton formula is equal to the Planck formula with an additional term, $h\nu/2k$, which represents an additional half-photon. This half-photon is the noise level from a body at absolute zero temperature and is referred to as the zero-point fluctuation noise. Figure 7.2 shows the relationships between physical temperature and noise temperature corresponding to the Rayleigh–Jeans, Planck, and Callen and Welton formulas, for a frequency of 230 GHz. Note that for the case of $h\nu/kT \ll 1$, we can put $\exp(h\nu/kT) - 1 \simeq (h\nu/kT) + \frac{1}{2}(h\nu/kT)^2$, in which case the Callen and Welton formula reduces to the Rayleigh–Jeans formula, but the result from the Planck formula is lower by $h\nu/2k$.

When using Eq. (7.3) to derive the noise temperature of a receiver, the values of T_{hot} and T_{cold} should be the noise temperatures derived from the Planck or Callen and Welton formulas, not the physical temperatures of the loads (except in the Rayleigh–Jeans domain). Thus, for the Planck formula, we can write

$$T_{R(\mathrm{Planck})} = \frac{T_{\mathrm{hot(Planck)}} - YT_{\mathrm{cold(Planck)}}}{Y - 1} \tag{7.8}$$

and a similar equation for the Callen and Welton formula. From Eqs. (7.4), (7.5), and (7.6), we obtain

$$T_{R(\text{Planck})} = T_{R(\text{C\&W})} + \frac{h\nu}{2k} \,. \tag{7.9}$$

In using any measurement of receiver noise temperature, it is important to know whether, in deriving it, the Planck formula, the Callen and Welton formula, or the physical temperature of the loads (i.e., the Rayleigh–Jeans approximation) was used. If the noise temperatures of the individual components are derived from the physical temperatures using the Callen and Welton formula, the temperature sum will be greater by $h\nu/2k$ than if the Planck formula were used; see Eq. (7.7). However, if the Callen and Welton formula is used to derive the receiver noise temperature, the result will be less by $h/2k$ than if the Planck formula were used; see Eq. (7.9). Thus the system temperature, which is the sum of the input temperature and the receiver temperature, will be the same whichever of the two formulas is used. However, to avoid confusion, it is important to use one formula or the other consistently throughout the derivation of the noise temperatures.

Differing opinions have been expressed on the nature of the zero-point fluctuation noise, and whether it should be considered as originating in the load connected to the receiver or in the receiver input stages; see, for example, Tucker and Feldman (1985), Zorin (1985), and Wengler and Woody (1987). At frequencies at which quantum effects become most important, the usual type of input stage in radio astronomy receivers is the SIS mixer, for which the quantum theory of operation is given by Tucker (1979). For a summary from various authors of some conclusions relevant to noise temperature considerations, see Kerr et al. (1997) and Kerr (1999).

To recapitulate: The radiation level predicted by the Callen and Welton formula is equal to the Planck radiation level plus the zero-point fluctuation component $h\nu/2$. The latter component is attributable to the power from a blackbody or matched resistive load at absolute zero temperature. An amplifier noise temperature derived using the Callen and Welton formula to interpret the measured Y factor is lower than that derived using the Planck formula by $h\nu/2k$. However, an antenna temperature obtained using the Callen and Welton formula is higher by $h\nu/2k$ than the corresponding Planck formula value. The system temperature, which is the sum of the noise temperature and the antenna temperature, is the same in either case. Since the system temperature determines the sensitivity of a radio telescope, these details may seem unimportant. However, in procuring an amplifier or mixer for a receiver input stage, it is important to know how the noise temperature is specified.

In addition to the noise generated in the electronics, the noise in a receiving system contains components that enter from the antenna. These components arise from cosmic sources, the cosmic background radiation, the Earth's atmosphere, the ground, and other objects in the sidelobes of the antenna. The opacity of the atmosphere, from which the atmospheric contribution to the system noise arises, is discussed in Chap. 13.

7.1.3 Local Oscillator

As explained in the previous chapter, local oscillator (LO) signals are required at the antenna locations and sometimes at other points along the signal paths to the correlators. The corresponding oscillator frequencies for different antennas must be maintained in phase synchronism to preserve the coherence of the signals. The phases of the oscillators at corresponding points on different antennas need not be identical, but the differences should be stable enough to permit calibration. Maintaining synchronism at different antennas requires transmitting one or more reference frequencies from a central master oscillator to the required points, where they may be used to phase-lock other oscillators. The frequencies required at the mixers can then be synthesized.

Special phase shifts are required at certain mixers to implement fringe rotation (fringe stopping), as described in Sect. 6.1, and to implement phase switching, as described in Sect. 7.5. Often these can best be synthesized by digital techniques, which can provide a signal at a frequency of, say, a few megahertz that contains the required frequency offsets and phase changes. These can be transferred to the LO frequency by using the synthesized signal as a reference frequency in a phase-locked loop.

7.1.4 IF and Signal Transmission Subsystems

After amplification in the low-noise front-end stages, the signals pass through various IF amplifiers and a transmission system before reaching the correlators. Transmission between the antennas and a central location can be effected by means of coaxial or parallel-wire lines, waveguide, optical fibers, or direct radiation by microwave radio link. Cables are often used for small distances, but for long distances, the cable attenuation may require the use of too many line amplifiers, and optical fiber, for which the transmission loss is much lower, is generally preferred. Low-loss TE_{01}-mode waveguide (Weinreb 1977b; Archer et al. 1980) was used in the construction of the original VLA system, which preceded the development of optical fiber by a few years. Optical fiber is now used for the Very Large Array (VLA)[1] (Perley et al. 2009). Cable or optical fiber can be buried at depths of 1–2 m to reduce temperature variations. Bandwidths of signals transmitted by cables are usually limited to some tens or hundreds of megahertz by attenuation, and radio links are similarly limited by available frequency allocations. For very wide bandwidths, optical fibers offer the greatest possibilities.

In the (mostly earlier) systems in which the signals are transmitted from the antennas to the central location in analog form, phase errors resulting from

[1] With the upgraded receiving system.

temperature effects in filters, and delay-setting errors, can be minimized by using the lowest possible intermediate frequency (IF) at this point. Accordingly, the final IF amplifiers may have a *baseband* response defined by a lowpass filter.[2] The response at the low-frequency end falls off at a frequency that is a few percent of the upper cutoff frequency.

7.1.5 Optical Fiber Transmission

The introduction of optical fiber systems provided a very great advance in transmission capability for broadband signals over long distances. Signals are modulated onto optical carriers, commonly in the wavelength range 1300–1550 nm, and transmitted along glass fiber. The fiber attenuation is a minimum of approximately 0.2 dB km^{-1} near 1550 nm and is about 0.4 dB km^{-1} at 1300 nm. These values are much lower than can be obtained in radio frequency transmission lines. In the fiber, a glass core is surrounded by a glass cladding of lower refractive index, so light waves launched into the core at a small enough angle with respect to the axis of the fiber can propagate by total internal reflection. If the inner-core diameter is approximately 50 μm, a number of different modes can be supported. These modes travel with slightly different velocities, which results in a limitation in performance of this multimode fiber. If the core is reduced to approximately 10 μm in diameter, only the HE_{11} mode propagates. Single-mode fiber of this type is required for the longest distances and/or the highest frequencies and bandwidths. At 1550 nm, an interval of 1 nm in wavelength corresponds to a bandwidth of approximately 125 GHz. The low attenuation and the bandwidth capacity facilitate the use of wide bandwidths and long baselines in linked-element arrays. Signals can be transmitted in analog form or digitized and transmitted as pulse trains. Design of a fiber transmission system involves the characteristics of the lasers that generate the optical carriers and the detectors that recover the modulation, as well as the characteristics of the fiber. For further information, see, for example, Agrawal (1992), Borella et al. (1997), and Perley et al. (2009).

In practice, the bandwidth and distance of the transmission are limited by the noise in the laser that generates the optical signal at the transmitting end of the fiber, and the noise in the diode demodulator and the amplifier at the receiving end. To avoid degradation of the sensitivity in analog transmission, the power spectral density of the signal (measured in W Hz^{-1}) must be greater than the power spectral density of the noise generated in the transmission system by $\sim$ 20 dB for most radio astronomy applications. However, the total signal power is limited by the need to avoid nonlinearity of the response of the modulator or demodulator. The result is a limit on the bandwidth of the signal, since for signals with a flat spectrum, the power

[2] In some cases, an image rejection mixer (see Appendix 7.1) is used for the conversion to baseband, but the suppression of the unwanted sideband may then be no greater than 20–30 dB.

is proportional to the bandwidth. In practice, a single transmitter and receiver pair can operate with a bandwidth of 10–20 GHz for transmission distances of some tens of kilometers. Optical amplifiers, which most commonly operate at wavelengths near 1550 nm, can be used to increase the range of transmission.

In the modulation process, the *power* of the carrier is varied in proportion to the *voltage* of the signal. Because of this, the effect of small unwanted components in fiber transmission systems is greatly reduced. Consider, for example, a small component of the optical signal resulting from a reflection within the fiber. If the optical power of the reflected component is x dB less than that of the main component, then after demodulation at the photodetector, the signal power contributed by the reflected component is $2x$ dB less than that from the main optical component. This also applies to small unwanted effects resulting from finite isolation of couplers, isolators, and other elements. Variations in the frequency response resulting from standing waves in microwave transmission lines are significantly less in optical fiber than in cable.

A feature that must be taken into account in applications of optical fiber is the dispersion in velocity, $\mathcal{D}$, usually specified in $\text{ps}(\text{nm} \cdot \text{km})^{-1}$. The difference in the time of propagation for two optical wavelengths that differ by $\Delta\lambda$ traveling a distance ℓ in the fiber is $\mathcal{D}\Delta\lambda\ell$. Figure 7.3 shows the dispersion for two types of fiber. Curve 1 is for a type of fiber widely used in early applications, and curve 2 represents a design in which the zero-dispersion wavelength is shifted to coincide approximately with the minimum-attenuation wavelength of 1550 nm. This optimization of the performance at 1550 nm is achieved by designing the fiber so that the dispersion of the cylindrical waveguide formed by the core of the fiber cancels the intrinsic dispersion of the glass at that wavelength.

Consider a spectral component, at frequency ν_m, of a broadband signal that is modulated onto an optical carrier. Amplitude modulation of the signal results in sidebands spaced $\pm\nu_m$ in frequency with respect to the carrier. Because of the velocity dispersion, the two sidebands and the carrier each propagate down the fiber with slightly different velocities and thus exhibit relative offsets in time at the receiving end. Such time offsets result in attenuation of the amplitude of the high-frequency components of analog signals and in broadening of the pulses used to represent digital data. Thus, for both analog and digital transmission, dispersion

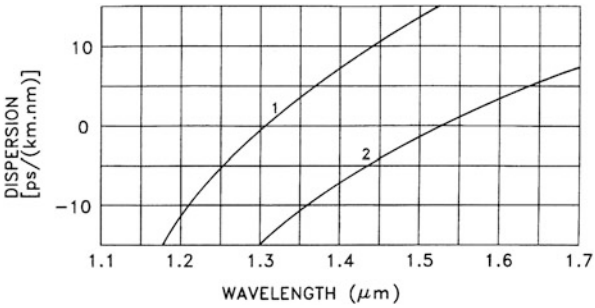

Fig. 7.3 Dispersion $\mathcal{D}$ in single-mode optical fiber of two different designs, as a function of the optical wavelength.

as well as noise can limit the bandwidth × distance product. An analysis of the effect of dispersion on analog signals is given in Appendix 7.2.

7.1.6 Delay and Correlator Subsystems

The compensating delays and correlators can be implemented by either analog or digital techniques. An analog delay system may consist of a series of switchable delay units with a binary sequence of values in which the delay of the nth unit is $2^{n-1}\tau_0$, where τ_0 is the delay of the smallest unit. Such an arrangement, with N units, provides a range of delay from zero to $(2^N - 1)\tau_0$ in steps of τ_0. For delays up to about 1 μs, lengths of coaxial cable or optical fiber have been used. The design of analog multiplying circuits for correlators has been discussed by Allen and Frater (1970). An example of a broadband analog correlator is described by Padin (1994). However, the development of digital circuitry capable of operating at high clock frequencies has led to the general practice of digitizing the IF signal so that the delay and correlators are generally implemented digitally, as discussed in Chap. 8.

7.2 Local Oscillator and General Considerations of Phase Stability

7.2.1 Round-Trip Phase Measurement Schemes

Synchronizing of the oscillators at the antennas can be accomplished by phase-locking them to a reference frequency that is transmitted out from a central master oscillator. Buried cables or fibers offer the advantage of the greatest stability of the transmission path. At a depth of 1–2 m, the diurnal temperature variation is almost entirely eliminated, but the annual variation is typically attenuated by a factor of 2–10 only. For a discussion of temperature variation in soil as a function of depth, see Valley (1965). As an example, a 10-km-long buried cable with a temperature coefficient of length of 10^{-5} K^{-1} might suffer a diurnal temperature variation of 0.1 K, resulting in a change of 1 cm in electrical length. A similar variation would occur in a 50-m length of cable running from the ground to the receiver enclosure on an antenna and subjected to a diurnal temperature variation of 20 K. Rotating joints and flexible cables can also contribute to phase variations.

Path length variations can be determined by monitoring the phase of a signal of known frequency that traverses the path. It is necessary for the signal to travel in two directions, that is, out from the master oscillator and back again, since the master provides the reference against which the phase must be measured. This technique is described as *round-trip phase measurement*. Correction for the measured phase changes can be implemented in hardware by using a phase shifter driven by the

measurement system, or in software by inserting corrections in the data from the correlator, either in real time or during the later stages of data analysis. It is also possible to generate a signal in which the phase changes are greatly reduced by combining signals that travel in opposite directions in the transmission line. As an illustration of the last procedure, consider a signal applied to the near end of a loss-free transmission line that results in a voltage $V_0 \cos(2\pi\nu t)$ at the far end. At a distance ℓ, measured back from the far end, the outgoing signal is $V_1 = V_0 \cos 2\pi\nu(t + \ell/v)$, where v is the phase velocity along the line. Suppose that the signal is reflected from the far end without change in phase. At the same point, distant ℓ from the far end, the returned signal is $V_2 = V_0 \cos 2\pi\nu(t - \ell/v)$, and the total signal voltage is

$$V_1 + V_2 = 2V_0 \cos(2\pi\nu t) \cos\left(\frac{2\pi\nu\ell}{v}\right) . \tag{7.10}$$

The first cosine function in Eq. (7.10) represents the radio frequency signal, the phase of which (modulo π) is independent of ℓ and of line length variations. The second cosine function is a standing-wave amplitude term. Such a system cannot easily be implemented in practice because of attenuation and unwanted reflections, and thus more complicated schemes have evolved. In what follows, we consider cable transmission, although the basic principles are applicable to other systems. Some general considerations, including the use of microwave links, are given by Thompson et al. (1968).

7.2.2 Swarup and Yang System

Several different round-trip schemes have been devised as instruments have developed, and one of the earliest of these was by Swarup and Yang (1961). A system based on this scheme is shown in Fig. 7.4. Part of the outgoing signal is reflected from a known reflection point at an antenna, and variation in the path length to the reflector is monitored by measuring the relative phase of the reflected component at the detector. The phase of the reflected signal is compared with that of a reference signal. The phase of the latter is variable by means of a movable probe that samples the outgoing signal. Since many other reflections may occur in the transmission line, it is necessary to identify the desired component. To do this, a modulated reflector, for example, a diode loosely coupled to the line, is used. This is switched between conducting and nonconducting states by a square wave voltage, and a synchronous detector is used to separate the modulated component of the reflected signal.

An increase $\Delta\ell$ in the length of the transmission line is detected as a corresponding movement of $2\Delta\ell$ in the probe position for the null. It results in an increase of $2\pi\Delta\ell\nu_1/v$ in the phase of the frequency ν_1 at the antenna, where v is the phase velocity in the line. The corresponding changes in LO phases and IF

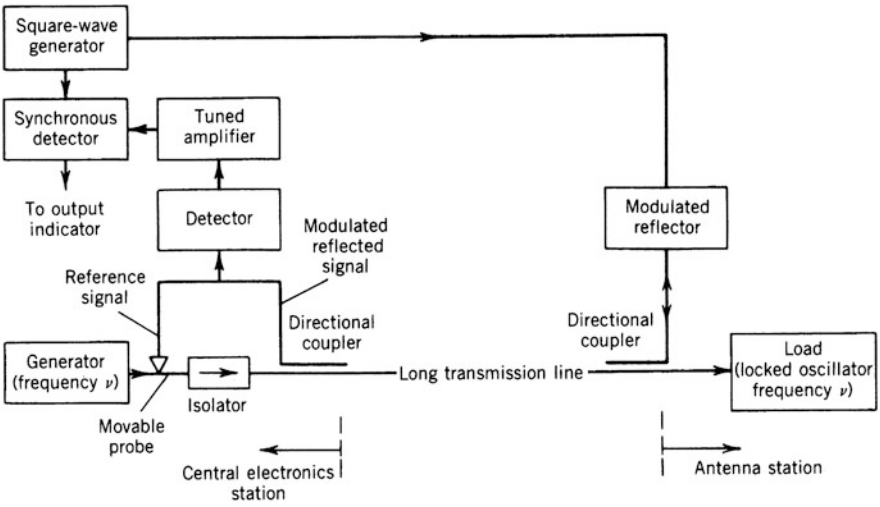

Fig. 7.4 System for measuring variations in the electrical path length in a transmission line, based on the technique of Swarup and Yang (1961). The output of the synchronous detector is a sinusoidal function of the difference between the phases of the reference (outgoing) and reflected components at the detector. A null output is obtained when these signal phases are in quadrature, and the position of the probe for a null is thus a measure of the phase of the reflected signal. Because of the isolator in the line, the probe samples only the outgoing component of the signal.

phases transmitted over the same path can be calculated and applied as a correction to the visibility phases.

7.2.3 Frequency-Offset Round-Trip System

A second scheme, shown in Fig. 7.5, is one in which the round-trip phase is measured directly. The signals traveling in opposite directions are at frequencies ν_1 and ν_2 that differ by only a small amount, but enough to enable them to be separated easily. This type of system is widely used, and we examine its performance in some detail. Note that although directional couplers or circulators allow the signals at the same frequency but going in opposite directions in the line to be separated, the signal from the unwanted direction is suppressed by only 20–30 dB relative to the wanted one. An unwanted component at a level of -30 dB can cause a phase error of 1.8°. However, the frequency offset enables the signals to be separated with much higher isolation.

An oscillator at frequency ν_2 at an antenna is phase-locked to the difference frequency of signals at ν_1 and $\nu_1 - \nu_2$, which travel to the antenna via a transmission line. The difference frequency $\nu_1 - \nu_2$ is small compared with ν_1 and ν_2. The

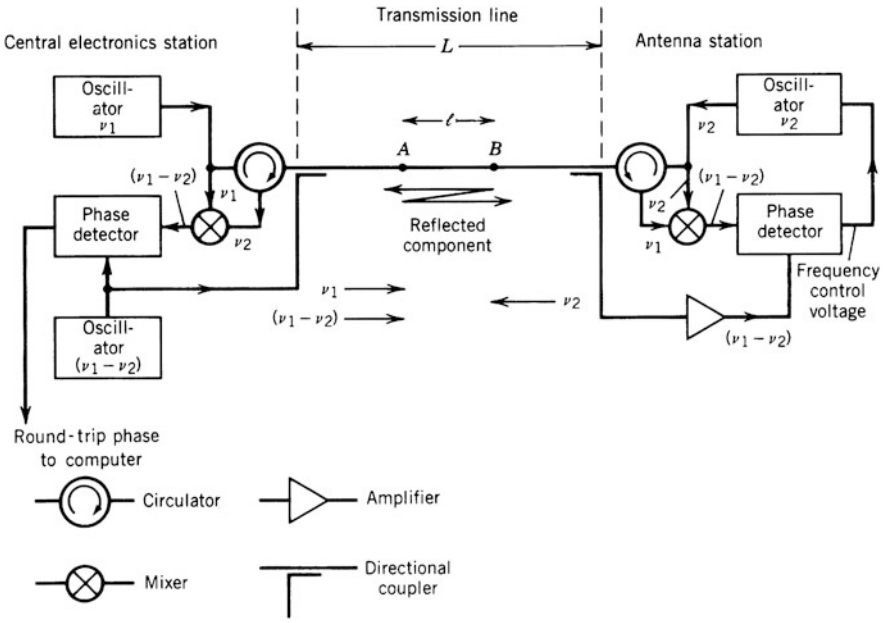

Fig. 7.5 Phase-lock scheme for the oscillator ν_2 at the antenna. Frequencies ν_1 and $\nu_1 - \nu_2$ are transmitted to the antenna station where they provide the phase reference to lock the oscillator. ν_1 and ν_2 are almost equal, so $\nu_1 - \nu_2$ is small. A signal at frequency ν_2 is returned to the central station for the round-trip phase measurement.

frequency ν_2 is returned to the master oscillator location for the round-trip phase comparison.

At the antenna, the phases of the signals at frequencies ν_1 and $\nu_1 - \nu_2$ relative to their phases at the central location are $2\pi\nu_1 L/v$ and $2\pi(\nu_1 - \nu_2)L/v$, where L is the length of the cable. The phase of the ν_2 oscillator at the antenna is constrained by a phase-locked loop to equal the difference of these phases, that is, $2\pi\nu_2 L/v$. The phase change in the ν_2 signal in traveling back to the central location is $2\pi\nu_2 L/v$, and thus the measured round-trip phase (modulo 2π) is $4\pi\nu_2 L/v$. Now suppose that the length of the line changes by a small fraction, β. The phase of the oscillator ν_2 at the antenna relative to the master oscillator changes to $2\pi\nu_2 L(1+\beta)/v$. The required correction to the ν_2 oscillator is just half the change in the measured round-trip phase. The problem that arises is that several effects, including reflections and velocity dispersion in the transmission line, can cause errors in the round-trip phase. Such errors result in phase offsets of the oscillator at the antenna, which is not serious if the offsets remains constant. However, in practice, it is likely to vary with ambient temperature. The largest error usually results from reflections, and control of this error places an upper limit on the difference frequency $\nu_1 - \nu_2$. We now examine this limit.

Consider what happens if reflections occur at points A and B separated by a distance ℓ along the line as in Fig. 7.5. The complex voltage reflection coefficients at these points are ρ_A and ρ_B, and their values will be assumed to be the same at frequencies ν_1 and ν_2. Signals ν_1 and ν_2, after traversing the cable, include components that have been reflected once at A and once at B. The coefficients ρ_A and ρ_B are sufficiently small that components suffering more than one reflection at each point can be neglected. For the frequency ν_1 arriving at the antenna, the amplitude (voltage) of the reflected component relative to the unreflected one is

$$\Lambda = |\rho_A||\rho_B|10^{-\ell\alpha/10} , \tag{7.11}$$

where α is the (power) attenuation coefficient of the cable in decibels per unit length. Note that the attenuation in voltage is equal to the square root of the attenuation in power. The phase of the reflected component relative to the unreflected one is (modulo 2π)

$$\theta_1 = 4\pi\ell\nu_1 v^{-1} + \phi_A + \phi_B , \tag{7.12}$$

where ϕ_A and ϕ_B are the phase angles of ρ_A and ρ_B (that is, $\rho_A = |\rho_A|e^{j\phi_A}$, etc.), and v is the phase velocity in the line. Figure 7.6 shows a phasor representation of the reflected and unreflected components and their phase θ_1. The reflected component causes the resultant phase to be deflected through an angle ϕ_1 given by

$$\phi_1 \simeq \tan\phi_1 = \frac{\Lambda \sin\theta_1}{1 + \Lambda\cos\theta_1} . \tag{7.13}$$

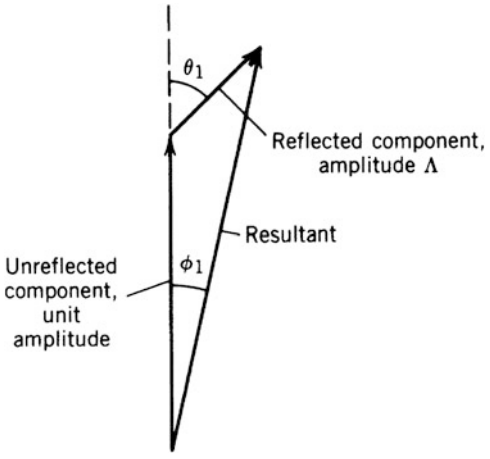

Fig. 7.6 Phasor diagram of components at frequency ν_1 transmitted by the cable.

Similarly, the phase of the frequency ν_2 is deflected through an angle ϕ_2, given by equations equivalent to Eqs. (7.12) and (7.13) with subscript 1 replaced by 2.

With the reflection effects represented by ϕ_1 and ϕ_2, the round-trip phase for a line of length L is

$$4\pi\nu_2 L v^{-1} + \phi_1 + \phi_2 \ . \tag{7.14}$$

If the line length increases uniformly to $L(1+\beta)$, the angles ϕ_1 and ϕ_2 vary in a nonlinear manner with ℓ and become $\phi_1 + \delta\phi_1$ and $\phi_2 + \delta\phi_2$, respectively. The round-trip phase then becomes

$$4\pi\nu_2 L v^{-1}(1+\beta) + \phi_1 + \delta\phi_1 + \phi_2 + \delta\phi_2 \ . \tag{7.15}$$

(The effect of the reflection on the phase of the signal at frequency $\nu_1 - \nu_2$ has been omitted since $\nu_1 - \nu_2$ is much smaller than ν_1 or ν_2, and reflections for the relatively low frequency may be very small. Also, the rate of change of phase of $\nu_1 - \nu_2$ with line length is correspondingly small.) The applied correction for the increase in line length is half the measured change in round-trip phase:

$$2\pi\nu_2\beta L v^{-1} + \frac{1}{2}(\delta\phi_1 + \delta\phi_2) \ . \tag{7.16}$$

However, the exact correction would be equal to the change in the phase of ν_2 at the antenna, which is

$$2\pi\nu_2\beta L v^{-1} + \delta\phi_2 \ . \tag{7.17}$$

Consequently, the phase correction is in error by

$$\frac{1}{2}(\delta\phi_1 + \delta\phi_2) - \delta\phi_2 = \frac{1}{2}(\delta\phi_1 - \delta\phi_2) \ . \tag{7.18}$$

If ν_1 and ν_2 were equal, the phase error would be zero. It is possible therefore to specify a maximum allowable difference frequency in terms of the maximum tolerable error.

The difference between the phase angles ϕ_1 and ϕ_2 is obtained from Eq. (7.13) as follows:

$$\begin{aligned}\phi_1 - \phi_2 &= \frac{\partial\phi_1}{\partial\nu_1}(\nu_1 - \nu_2) \\ &= \frac{4\pi\ell v^{-1}\Lambda\cos\theta_1(1+\Lambda\cos\theta_1) + 4\pi\ell v^{-1}\Lambda^2\sin^2\theta_1}{(1+\Lambda\cos\theta_1)^2}(\nu_1 - \nu_2) \ .\end{aligned} \tag{7.19}$$

The reflected amplitude Λ must be much less than unity if phase errors are to be tolerable, so terms in Λ^2 can be omitted from the numerator in Eq. (7.19), and the denominator is approximately unity. Thus,

$$\phi_1 - \phi_2 \simeq 4\pi \ell v^{-1} \Lambda(\nu_1 - \nu_2) \cos\theta_1 \ . \tag{7.20}$$

The variation of $\phi_1 - \phi_2$ with line length is given by

$$\begin{aligned} \delta\phi_1 - \delta\phi_2 &= \beta\ell \frac{\partial}{\partial \ell}(\phi_1 - \phi_2) \\ &= 4\pi v^{-1} \Lambda \left[\cos\theta_1 - 0.1\ell\alpha(\ln 10)\cos\theta_1 - 4\pi v^{-1}\ell\nu_1 \sin\theta_1\right] \\ &\quad \times (\nu_1 - \nu_2)\beta\ell \ . \end{aligned} \tag{7.21}$$

The maximum values of the terms in square brackets in Eq. (7.21) are dominated by the third term, which is of the order of the number of wavelengths in the line. If the two smaller terms are neglected, we obtain the magnitude of the phase error as follows:

$$\frac{1}{2}(\delta\phi_1 - \delta\phi_2) \simeq 8\pi^2 v^{-2} |\rho_A||\rho_B| \beta \ell^2 10^{-\alpha\ell/10} \nu_1(\nu_1 - \nu_2) \sin\theta_1 \ . \tag{7.22}$$

The factor $\ell^2 10^{-\alpha\ell/10}$ has a maximum value at

$$\ell = 20(\alpha \ln 10)^{-1} \ . \tag{7.23}$$

This maximum occurs because for small values of ℓ, the change in the angle θ with frequency or cable expansion is small, and for large values of ℓ, the reflected component is greatly attenuated. The maximum value is equal to

$$\left[\ell^2 10^{-\alpha\ell/10}\right]_{\max} = 10.21\alpha^{-2} \ . \tag{7.24}$$

Curves of $\ell^2 10^{-\alpha\ell/10}$ are plotted in Fig. 7.7 for various values of α that correspond to good-quality cables. It is evident that reducing the attenuation in a cable increases the error in the round-trip phase correction in Eq. (7.22).

The type of reflections that may be encountered depends on the type of transmission line and how it is used. For example, consider a buried coaxial cable that runs along a set of stations used for a movable antenna. The principal cause of reflections in such a cable is the connectors that are inserted at the antenna stations. Unless the antenna is at the closest station, there are one or more interconnecting loops, where unused stations are bypassed, between the antenna and the master oscillator. If there are n connectors in the cable, there are $N = n(n-1)/2$ pairs between which reflections can occur. Also, if the phasors of the corresponding reflected components combine randomly, the overall rms error in the phase correction is, from Eq. (7.22),

$$\delta\phi_{\text{rms}} = \sqrt{32}\pi^2 v^{-2} |\rho|^2 \beta \nu_1(\nu_1 - \nu_2) F(\alpha, \ell) \ , \tag{7.25}$$

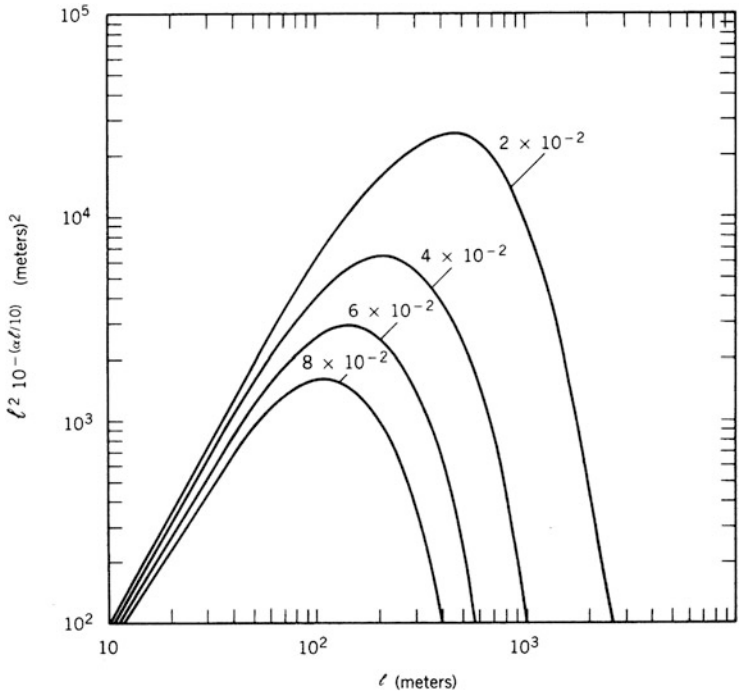

Fig. 7.7 The function $\ell^2 10^{-\alpha\ell/10}$ plotted against ℓ for four values of the transmission-line attenuation, α dB m^{-1}. This function is a factor in the round-trip phase error given by Eq. (7.22).

where

$$F(\alpha, \ell) = \sqrt{\sum_{i=1}^{n} \sum_{k<i} \ell_{ik}^4 10^{-2\alpha\ell_{ik}/10}}\,, \tag{7.26}$$

the rms value has been used for sin θ_1, and the reflection coefficients are all approximated by an average magnitude $|\rho|$.

As an example, suppose that an interferometer is designed for observations near 100 GHz and that it incorporates ten antenna stations in a linear configuration at approximately equal increments in distance up to 1 km from the master oscillator. The interconnecting oscillator cable carries a reference signal at $\nu_1 = 2$ GHz, and for this cable $|\rho| = 0.1, \alpha = 0.06$ dB m^{-1}, $v = 2.4 \times 10^8$ ms^{-1}, and the temperature coefficient of electrical length is 10^{-5} K^{-1}. From Eq. (7.26), we find that $F(\alpha, \ell) = 1.1 \times 10^4$. For a temperature variation of 0.1 K in the cable, $\beta = 10^{-6}$. If phase errors at 100 GHz are required to be less than 1°, $\delta\phi_{\text{rms}}$ must not exceed 0.02°, and from Eq. (7.25), ν_1 and ν_2 must not differ by more than 1.6 MHz.

7.2.4 *Automatic Correction System*

An interesting variation on the round-trip scheme, shown in Fig. 7.8, was suggested by J. Granlund (National Radio Astronomy Observatory 1967). It is particularly suitable for providing a stable reference frequency at a number of points along a linear array of antennas. Frequencies ν_1 and ν_2 are generated by stable oscillators and are injected at opposite ends of the transmission line. The difference frequency $\nu_1 - \nu_2$ is again very small. At an intermediate station, the two signals are extracted by directional couplers and multiplied to form the sum frequency. The phase of this sum at the antenna station in Fig. 7.8 is

$$2\pi\nu_1\ell_1 v^{-1} + 2\pi\nu_2(L-\ell_1)v^{-1} = 2\pi\nu_1 L v^{-1} - 2\pi(\nu_1-\nu_2)(L-\ell_1)v^{-1} \,. \qquad (7.27)$$

For two points at positions ℓ_1 and ℓ_2 on the line, the difference in the sum-frequency phases is

$$\Delta\phi = 2\pi(\nu_1-\nu_2)(\ell_1-\ell_2)v^{-1} \,. \qquad (7.28)$$

This difference would be zero if ν_1 and ν_2 were equal, but it is necessary to maintain a finite difference frequency because the directivity of the couplers alone is seldom sufficient to separate the two signals adequately. The effect of the line length variation is not measured explicitly in this case, but the correction occurs automatically, except for the small term in Eq. (7.28). Reflections in the cable can

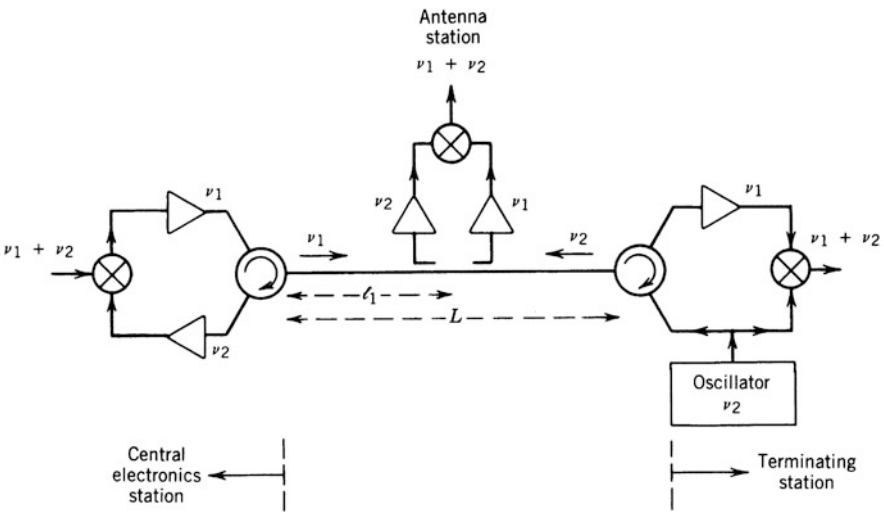

Fig. 7.8 Scheme proposed by J. Granlund (National Radio Astronomy Observatory 1967) for establishing a reference signal at frequency $\nu_1 + \nu_2$ at various stations along a transmission line. One such antenna station is shown.

produce errors, as described for the previous scheme, and may be the limiting consideration for the frequency offset. A practical implementation of the scheme of Fig. 7.8 is described by Little (1969).

7.2.5 *Fiberoptic Transmission of LO Signals*

Optical fiber can replace cables and transmission lines in most of the LO schemes discussed above. Some features of optical fiber transmission that should be taken into account are outlined below.

- Different optical wavelengths can be used in the two directions of a round-trip system to help separate the signals. At the antenna, the frequency of the laser signal from the master LO can be offset by a few tens of megahertz by using a special modulating device, and injected into the line in the return direction. Alternately, a different laser can be used for the return signal. It is important to take into account the effects of the fiber dispersion and temperature-induced changes in the laser wavelengths, particularly in the case in which two different lasers are used. However, if the laser wavelengths are chosen to be very close to the zero-dispersion wavelength of the fiber, the resulting errors can be minimized.
- As mentioned in Sect. 7.1, the performance of optical components such as isolators and directional couplers is much better than that of corresponding microwave components. With careful design, it is possible to use such components to separate signals at the same laser wavelength traveling in opposite directions in a fiber. Round-trip phase systems have been made in which a radio frequency signal is transmitted on an optical carrier, and at the receiving end, a half-silvered mirror is used to return a component of the signal back along the fiber for a round-trip measurement. It may be necessary to use an optical isolator at the transmitting end to ensure that any of the returned signal that reaches the laser is very small. Reflection of a laser signal back into the output can disturb the operation of the laser.
- In general, when a multifiber cable is flexed, the effective lengths of the individual fibers vary smoothly and remain matched to a much greater degree than is the case for bundled coaxial cables. As a result, it may be possible to use two separate fibers for the two different directions in a round-trip scheme, depending on the accuracy required.
- Twisting of a straight fiber that is held under constant tension has been found to cause less change in the electrical length than bending of a fiber. Twisting, however, can result in small changes in the amplitude of the transmitted signal, resulting from the residual sensitivity of the optical receiver to the angle of the linear polarization of the light.
- It is possible to stabilize the length of the path through a fiber by use of round-trip phase measurement at the optical wavelength. In practice, this requires the use of an automatic correction loop in which a length adjustment device is

controlled by the round-trip phase, since length variations comparable to the optical wavelength can occur on timescales of much less than one second.

- An LO frequency can be transmitted as the difference frequency of two optical laser signals that travel in the same fiber. The radio frequency is generated by combining the optical signals in a photo-optic diode. Radio power of several microwatts can be obtained, which is sufficient to provide LO power for an SIS mixer. This scheme is particularly attractive for receivers at millimeter and submillimeter wavelengths (Payne et al. 1998).
- For standard optical fiber, the temperature coefficient of length is approximately 7×10^{-6} K^{-1}. High-stability fiber, developed by Sumitomo for special applications, has a temperature coefficient that is about an order of magnitude less and was used in the Submillimeter Array without a round-trip correction system (Moran 1998).

7.2.6 Phase-Locked Loops and Reference Frequencies

Some practical points in the implementation of LO systems should be briefly mentioned. In two of the schemes described above, an oscillator at the antenna is controlled by a phase-locked loop. Details of the design of phase-locked loops are given, for example, by Gardner (1979), and here we mention only the choice of the natural frequency of the loop. Unless the natural frequency is about an order of magnitude less than the frequency at the inputs of the phase detector, the loop response may be fast enough to introduce undesirable phase modulation at the phase detector frequency. In the system in Fig. 7.5, the frequency of the input signals to the phase detector is the offset frequency $\nu_1 - \nu_2$, an upper limit on which has been placed by consideration of the reflections in the line. Also, the bandwidth of the noise to which the loop responds is proportional to the natural frequency. These considerations place an upper limit on the natural frequency of the loop, which in turn limits the choice of the oscillator to be locked. An oscillator with inherently poor phase stability (when unlocked) requires a loop with a higher natural frequency than does a more stable oscillator. Crystal-controlled oscillators are highly stable and require loop natural frequencies of only a few hertz. They are especially suitable for long transmission lines because the noise bandwidth of the loop is correspondingly small. With crystal-controlled oscillators at the antennas, it is possible to send out the reference frequency in bursts, rather than continuously. Signals traveling in opposite directions can then be separated by time multiplexing, and no frequency offset is required. However, the change in impedance of the circuits at the ends of the cable when the direction of the signal is reversed could become a limiting factor in the accuracy of the round-trip phase measurement. Systems of this type have been designed for several large arrays (Thompson et al. 1980; Davies et al. 1980).

In addition to the establishment of a phase-locked oscillator at each antenna at a reference frequency (equal to ν in Fig. 7.4, ν_2 in Fig. 7.5, and $\nu_1 + \nu_2$ in

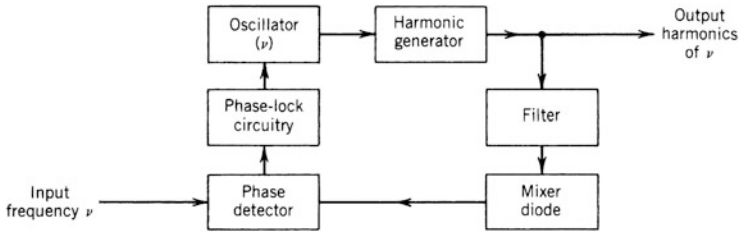

Fig. 7.9 Scheme for generating a comb spectrum of harmonics of a frequency ν, in which phase changes in the harmonic generator are eliminated by enclosing it within a phase-locked loop. The filter passes two harmonics that combine in the mixer diode to generate a signal at frequency ν.

Fig. 7.8), it is necessary to generate the multiples or submultiples of this frequency that are required for frequency conversions of the received signal. In frequency multiplication, phase variations increase in proportion to the frequency. Within the multiplier chain from the frequency standard to the first LO frequency, the choice of frequency that is transmitted from the central location to the antenna is generally not critical. However, if significant noise is added in the transmission process, it may be better to transmit a high frequency to minimize multiplication of phase errors resulting from the added noise.

Minimization of phase variations in the frequency-multiplication circuit is largely a matter of reducing temperature-related effects, and in this regard, the scheme depicted in Fig. 7.9 is worthy of mention. It may be useful to generate a "comb" spectrum consisting of many harmonics that can be used, for example, for tuning in discrete frequency intervals. This can be done by applying the fundamental frequency to a varactor diode, but the voltage at which the varactor goes into conduction varies with temperature, so the phase of the waveform at which it starts to conduct during each cycle varies. This causes variation in the phases of the harmonics that are generated. In the circuit in Fig. 7.9, the effect of this variation is eliminated. The input fundamental waveform at frequency ν is not applied directly to the harmonic generator but is used to lock an oscillator at frequency ν. This oscillator drives the harmonic generator. The waveform at the oscillator frequency that is compared with the input frequency is taken after the varactor by selecting two adjacent harmonics and combining them in a mixer diode. The phase-locked loop holds constant the phase of this output waveform relative to the input frequency ν and adjusts the phase of the oscillator to compensate for a change in time of switch-on of the varactor.

In the case of a connected-element array, low-frequency components of the phase noise of the master oscillator cause similar effects in the LO phase at each antenna, and therefore their contributions to the relative phase of the signals at the correlator input tend to cancel. However, the frequency components of the phase noise suffer phase changes as a result of the time delay in the path of the reference signal from the master oscillator to each antenna, and also as a result of the time delay of the IF signal from the corresponding mixer to the correlator input (including the variable delay that compensates for the geometric delay). Thus, the cancellation is

important only for frequency components of the phase noise that are low enough that differences in these phase changes, from one antenna to another, are small. The bandwidths of phase-locked loops in the LO signals can also limit the frequency range over which phase noise in the master oscillator is canceled. In practice, cancellation of phase noise from the master oscillator is likely to be effective up to a frequency in the range of some tens of hertz to a few hundred kilohertz, depending upon the parameters of the particular system.

7.2.7 Phase Stability of Filters

Tuned filters used for selecting LO frequencies are also a source of temperature-related phase variations. The phase response ϕ of a filter changes by approximately $n\pi/2$ across the 3-dB bandwidth $\Delta\nu$, where n is the number of sections (poles). Thus, the rate of change of phase with frequency, measured at the center frequency ν_0, is

$$\left.\frac{\partial\phi}{\partial\nu}\right|_{\nu_0} = \frac{n\pi k_1}{2\Delta\nu} , \tag{7.29}$$

where k_1 is a constant of order unity that depends on the design of the filter. The center frequency varies with physical temperature T by

$$\frac{\partial\nu_0}{\partial T} = k_2\nu_0 , \tag{7.30}$$

where k_2 is a constant related to the coefficients of expansion and variation of the dielectric constant of the filter. Thus, the rate of variation of phase with temperature is given by

$$\frac{\partial\phi}{\partial T} = \left.\frac{\partial\phi}{\partial\nu}\right|_{\nu_0} \frac{\partial\nu_0}{\partial T} = nk_1k_2\left(\frac{\pi}{2}\right)\left(\frac{\nu_0}{\Delta\nu}\right) . \tag{7.31}$$

The factor $\nu_0/\Delta\nu$ is the Q-factor of the filter. The combined constant k_1k_2 can be determined empirically and is typically of order 10^{-5} K^{-1} for tubular bandpass filters with center frequencies in the range 1 MHz to 1 GHz. Thus, for example, if one allows a 1-K temperature variation for such a filter and places an upper limit of 0.1° on its contribution to the phase variation, the fractional bandwidth must not be less than $n/100$, or 5.4%, for a six-pole filter. Filters of narrow fractional bandwidth should be used with caution. To pick out a particular frequency from a series of closely spaced harmonics, it may be preferable to use a phase-locked oscillator rather than a filter.

7.2.8 *Effect of Phase Errors*

Rapidly varying phase errors, such as those resulting from noise in LO circuits, cause a loss in signal amplitude and hence in sensitivity. They may also cause errors in the visibility phase, but the effect is small, since fast variations in the visibility phase are substantially reduced by the visibility averaging. To determine the loss in sensitivity, the signals from two antennas can be represented by $V_m e^{\phi_m(t)}$ and $V_n e^{\phi_n(t)}$ at the correlator inputs, where the ϕ terms are the phase errors for antennas m and n. The correlator output is

$$r = \langle V_m e^{\phi_m(t)} V_n^* e^{\phi_n(t)} \rangle \ , \tag{7.32}$$

where the angle brackets represent the expectation. Then if $\Delta\phi = [\phi_m(t) - \phi_n(t)]$ is the phase error, we have

$$r = V_m V_n^* [\langle \cos \Delta\phi \rangle + j \langle \sin \Delta\phi \rangle] \ . \tag{7.33}$$

If the probability distribution of $\Delta\phi$ is an even function with zero mean, which is frequently the case, the time average of the sine term has an expectation of zero. Then, by using the first two terms of the series expression for a cosine, we obtain a result in terms of the rms phase error, $\Delta\phi_{\rm rms}$:

$$r \simeq [1 - \frac{1}{2} \Delta\phi_{\rm rms}^2] \ . \tag{7.34}$$

The cosine approximation is accurate to 1% for values of $\Delta\phi_{\rm rms}$ less than $\sim 37°$. A reduction in sensitivity of 1% occurs for $\Delta\phi_{\rm rms} = 8.1°$.

7.3 Frequency Responses of the Signal Channels

7.3.1 *Optimum Response*

The signals in a synthesis array may pass through amplifiers, filters, and mixers before being converted to digital form. The characteristics of these components can vary with temperature, etc. However, the resulting problems have become less serious as improvements in the technology allow digitization to take place at earlier stages in the receiving system. Also, for systems with multichannel correlators, as used for spectral line observations, gains of the individual channels can be adjusted to provide a uniform response across the full receiving band. However, it is important to consider the effect of gain variations in analog components since low-noise input stages are generally followed by further amplification to increase the signal levels to something of order 20 dbm or more before they are digitized.

Except in cases in which the astronomical signals cover a wide relative bandwidth, the signal and the receiver noise both have largely flat spectra over the width of an IF band, and the broad spectral limits of the signal delivered to the digitizer, or, in earlier systems, to the analog correlator, are determined by the frequency response of the receiving equipment. If $H(\nu) = |H(\nu)|e^{j\phi(\nu)}$ is the voltage–frequency response function, the output from the correlator for antennas m and n, resulting from cosmic signals, is proportional to

$$\frac{1}{2}\int_{-\infty}^{\infty} H_m(\nu)H_n^*(\nu)\,d\nu = \mathcal{R}e\left[\int_0^{\infty} H_m(\nu)H_n^*(\nu)\,d\nu\right]$$
$$= \mathcal{R}e\left[\int_0^{\infty} |H_m(\nu)||H_n(\nu)|e^{j(\phi_m-\phi_n)}d\nu\right], \qquad (7.35)$$

where we have used the relation in Eq. (A3.6) of Appendix 3.1, $H_mH_n^*$ being Hermitian, and the subscripts denote the antennas. We are concerned here with the dependence of the signal-to-noise ratio (SNR) of an observation on the frequency responses of the signal channels. In practice, the frequency responses are nonzero only within a limited frequency band of width $\Delta\nu$. From Eq. (6.42), we can define a factor $\mathcal{F}$ equal to the SNR relative to that with identical rectangular responses of width $\Delta\nu$:

$$\mathcal{F} = \frac{\mathcal{R}e\left[\int_0^{\infty} H_m(\nu)H_n^*(\nu)\,d\nu\right]}{\sqrt{\Delta\nu\int_0^{\infty} |H_m(\nu)|^2\,|H_n(\nu)|^2\,d\nu}}. \qquad (7.36)$$

This equation has a maximum value if $|H_m(\nu)|$ and $|H_n(\nu)|$ are constant across the band $\Delta\nu$, that is, if the amplitude response is a rectangular function. If, in addition, $\phi(\nu)$ is identical for both antennas, $\mathcal{F}$ is equal to unity. Thus, a rectangular passband yields the greatest sensitivity within a limited bandwidth. Note that the same integral of $H_mH_n^*$ applies to both the real and imaginary parts of a complex correlator, and hence it also applies to the modulus of the visibility.

Of the other ways in which the receiving passband modifies the response of a synthesis array, the most important is the smearing of detail in the synthesized response, which limits the field of view that can usefully be imaged. This effect has been described in Sect. 6.3. For a given sensitivity, a rectangular passband results in the least smearing, since it is the most compact in the frequency dimension.

An exact rectangular passband is only an ideal concept. In practice, the steepness of the sides of the passband must be determined by the particular design and the number of poles in the response. The response can be made to approximate a rectangular shape more closely as the number of poles increases, with a proportionate increase in $\partial\phi/\partial T$ as shown by Eq. (7.31). To examine the tolerable deviations of the actual passband responses, two effects must be considered: the decrease in the SNR,

and the introduction of errors in determining gain factors for individual antennas, as will be described.

7.3.2 *Tolerances on Variation of the Frequency Response: Degradation of Sensitivity*

We first consider the effects on the sensitivity. Equation (7.36) provides a degradation factor $\mathcal{F}$, which is the SNR with frequency responses $H_m(\nu)$ and $H_n(\nu)$, expressed as a fraction of that which would be obtained with rectangular passbands of width $\Delta(\nu)$. In constructing a receiving system, the usual goal is to keep the passband flat with steep edges, but in practice, effects such as differential attenuation and reflections in cables introduce slopes and ripples in the frequency response that are not identical from one antenna to another. To examine these effects, $\mathcal{F}$ can be calculated for an initially rectangular passband with various distortions imposed. The distortions considered are the following:

1. Amplitude slope across the passband, with the logarithm of the amplitude varying linearly with frequency.
2. Sinusoidal amplitude ripple; this could result from a reflection in a transmission line.
3. Displacement of the center frequency of the passband.
4. Variation in phase response as a function of frequency.
5. Delay-setting error, which introduces a component of phase linear with frequency.

The first four of these effects apply mainly to signals in analog form and so are of most importance in systems of earlier design in which digitization of the signals occurred only in the later stages. Expressions for the frequency response involving the above effects are given in the first column of Table 7.1. The second column of the table gives the signal-to-noise degradation factor $\mathcal{F}$, and subscripts m and n indicate parameter values for particular antennas. The expressions in Table 7.1 have been used to derive the maximum tolerable passband distortion for each of the effects, allowing a loss in sensitivity of no more than 2.5% ($\mathcal{F} = 0.975$). The resulting limits on the passband distortion are shown in Table 7.2. A discussion of limits with more stringent tolerances associated with the ALMA array is given by D'Addario (2003).

Table 7.1 Deviation of the frequency characteristic from an ideal rectangular response, and corresponding expressions for $\mathcal{F}$ and G_{mn}

Frequency response	Signal-to-noise degradation, $\mathcal{F}$	Antenna-pair gain, G_{mn}
Amplitude slope[a]		
$\lvert H(\nu)\rvert^2 = H_0^2 e^{\sigma(\nu-\nu_0)} \prod\left(\frac{\nu-\nu_0}{\Delta\nu}\right)$	$\sqrt{\frac{4\left[e^{(\sigma_m+\sigma_n)\Delta\nu/2}-1\right]}{\Delta\nu(\sigma_m+\sigma_n)\left[e^{(\sigma_m+\sigma_n)\Delta\nu/2}+1\right]}}$	$\frac{2G_0}{\Delta\nu(\sigma_m+\sigma_n)}\left[e^{(\sigma_m+\sigma_n)\Delta\nu/4}-e^{-(\sigma_m+\sigma_n)\Delta\nu/4}\right]$
Sinusoidal ripple		
$H(\nu) = H_0\left[1+\gamma e^{j2\pi(\nu-\nu_0)\tau}\right]\prod\left(\frac{\nu-\nu_0}{\Delta\nu}\right)$	$\left[\frac{1+2\mathcal{R}e\left\{\gamma_m\gamma_n^*\right\}+\lvert\gamma_m\gamma_n\rvert^2}{1+\lvert\gamma_m\rvert^2+\lvert\gamma_n\rvert^2+2\mathcal{R}e\left\{\gamma_m\gamma_n^*\right\}+\lvert\gamma_m\gamma_n\rvert^2}\right]^{1/2}$ (see footnote b)	$G_0\left[1+\frac{2}{\pi}(\gamma_m+\gamma_n^*)+\gamma_m\gamma_n^*\right]$ (see footnote c)
Center-frequency displacement[d]		
$H(\nu) = H_0\prod\left(\frac{\nu-\delta\nu-\nu_0}{\Delta\nu}\right)e^{jN\pi(\nu-\delta\nu-\nu_0)/\Delta\nu}$	$\sqrt{1-\frac{\delta\nu_m-\delta\nu_n}{\Delta\nu}}$	$G_0\left[1-\frac{\delta\nu_m-\delta\nu_n}{\Delta\nu}\right]e^{jN\pi(\delta\nu_m-\delta\nu_n)/\Delta\nu}$
Phase variation		
$H(\nu) = H_0\prod\left(\frac{\nu-\nu_0}{\Delta\nu}\right)e^{j\phi(\nu)}$	$1-\frac{1}{2}\langle\phi_{mn}^2\rangle$ $\phi_{mn}(\nu) = \phi_m(\nu)-\phi_n(\nu)-\langle\phi_m(\nu)-\phi_n(\nu)\rangle$ (see footnote e)	$G_0\left[1-\frac{1}{2}\langle\phi_{mn}^2\rangle\right]$
Delay-setting error		
$H(\nu) = H_0 e^{j2\pi\nu\tau}\prod\left(\frac{\nu-\nu_0}{\Delta\nu}\right)$	$\frac{\sin\left[\pi\Delta\nu(\tau_m-\tau_n)\right]}{\pi\Delta\nu(\tau_m-\tau_n)}$	$G_0\left[\frac{\sin\pi\Delta\nu(\tau_m-\tau_n)}{\pi\Delta\nu(\tau_m-\tau_n)}\right]e^{j\pi\Delta\nu(\tau_m-\tau_n)}$ (see footnote f)

[a]The unit rectangle function $\prod(x)$ is equal to 1 for $\lvert x\rvert \le \frac{1}{2}$ and zero for $\lvert x\rvert > \frac{1}{2}$. Parameters are as follows: H_0 and G_0, gain constants; σ, slope parameter; ν_0, passband center frequency; γ, relative amplitude of sinusoidal component; $\delta\nu$, frequency offset; τ, delay error.
[b]For integral value of $\Delta\nu\tau$ (integral number of cycles across passband).
[c] $\Delta\nu\tau = \frac{1}{2}$ (half cycle of sinusoidal ripple across passband).
[d]Linear phase response with difference $N\pi$ between passband edges.
[e]The brackets $\langle\ \rangle$ indicate a mean over the passband.
[f]Phase term corresponds to baseband response (center frequency $= \Delta\nu/2$).

Table 7.2 Examples of frequency response tolerances

	Criterion	
Type of variation	2.5% Degradation in Signal-to-noise ratio	1% Maximum Gain error
Amplitude slope	3.5 dB edge-to-edge	2.7 dB edge-to-edge
Sinusoidal ripple	2.9 dB peak-to-peak	2.0 dB peak-to-peak
Center-frequency displacement	$0.05\Delta\nu$	$0.007\Delta\nu$
Phase variation	$\phi_{mn} = 12.8°$ rms	$\phi_{mn} = 9.1°$ rms
Delay-setting error	$0.12/\Delta\nu$	$0.05/\Delta\nu$

7.3.3 *Tolerances on Variation of the Frequency Response: Gain Errors*

A second effect that sets limits on the deviations of the frequency responses results from errors that can be introduced in the calibration procedure. If we omit the noise terms, the output of the correlator for an antenna pair can be expressed as

$$r_{mn} = G_{mn}\mathcal{V}_{mn} \ , \tag{7.37}$$

where $\mathcal{V}_{mn}$ is the source-dependent complex visibility from which the intensity map can be computed, and G_{mn} is a gain factor related to the frequency responses of the signal channels. We suppose that these responses incorporate the characteristics of the antennas and electronics in such a way that G_{mn} is proportional to the correlator output for antenna pair (m, n) when a point source of unit flux density at the field center is observed. In practice, the G_{mn} values may be determined from observations of calibration sources for which the visibilities are known. The measured antenna-pair gains can be used to correct the correlator output data directly, but there are advantages if, instead, they are used to determine (voltage) gain factors $g = |g|e^{j\phi}$ for the individual antennas such that

$$G_{mn} = g_m g_n^* \ . \tag{7.38}$$

Since, in a large array, there are many more correlated antenna pairs than antennas [up to $n_a(n_a - 1)/2$ pairs for n_a antennas], not all the calibration data need be used. This adds important flexibility to the calibration procedure; for example, a source resolved at the longest spacings of an array can be used to determine the antenna gains from measurements made only at the shorter spacings. The same principle leads to adaptive calibration described in Sect. 11.3.

In general, the factoring in Eq. (7.38) requires that the frequency responses be identical for all antennas or differ only by constant multiplicative factors. If this requirement is fulfilled, we can assign gain factors

$$g = \sqrt{\int_0^\infty |H(\nu)|^2 d\nu} \ . \tag{7.39}$$

In practice, the frequency responses differ, and an approximate solution to Eq. (7.38) can be obtained by choosing the g values to minimize

$$\sum |G_{mn} - g_m g_n^*|^2 \,, \tag{7.40}$$

where the summation is taken over all antenna pairs (m, n) for which G_{mn} can be measured by observation of a calibration source. In calibrating subsequent observations of unknown sources, $g_m g_n^*$ is used in place of G_{mn} in Eq. (7.37) for all antenna pairs, whether they are directly calibrated or not. To avoid introducing errors with this scheme, the residuals

$$\varepsilon_{mn} = G_{mn} - g_m g_n^* \tag{7.41}$$

must be small, which requires that the frequency responses be sufficiently similar. Thus, we are concerned here with the deviations of the frequency responses from one another rather than from an ideal response.

By using model responses for groups of antennas—calculating the pair gains, the best-fit antenna gains, and the residuals—tolerances on the bandpass distortion can be assigned. Pair gains for the various distortions discussed earlier are given in the third column of Table 7.1. Table 7.2 shows examples of tolerances. The results depend to some extent on the distribution of distortions in the model responses, which for the results shown were chosen with the intention of maximizing the residuals. The criteria of 2.5% loss in sensitivity and 1% maximum gain error shown in Table 7.2 were used during the early operation of the VLA (Thompson and D'Addario 1982). More stringent criteria may be appropriate, depending on the sensitivity and dynamic range to be achieved. The acceptable level of gain error for any instrument can be determined by making calculations of the response to source models with simulated errors of various levels introduced into the model visibility data. Bagri and Thompson (1991) give a discussion of the sources and effects of gain errors in the VLA.

7.3.4 Delay and Phase Errors in Single- and Double-Sideband Systems

For an incoming wavefront from a source, the path lengths to different antennas of an array are generally unequal. The relative time differences in the wavefront arrival at the antennas are referred to as the geometric delays, τ_g. To compensate for the different geometric delays, the signal received at each antenna is subjected to an instrumental delay τ_i that is continuously adjusted so that $\tau_g + \tau_i$ is the same for all antennas. Thus, the signals at the correlator inputs are aligned in time with respect to a common wavefront incident from the phase reference position. The fringes at the correlator output result from the fact that the signals traverse the geometric and

the instrumental delays at different frequencies and that the phase shifts resulting from the delays vary as the delays themselves change. In an ideal situation, the instrumental delays would be continuously adjusted, and if there were no frequency changes within the receivers, no fringe oscillations would occur. In practice, the situation is rather more complicated. The instrumental delays are inserted after the signals have been digitized, and the sample interval τ_s provides a convenient unit for coarse adjustment. For Nyquist sampling, $\tau_s = 1/2\Delta\nu$, where $\Delta\nu$ is the signal bandwidth.

7.3.5 Delay Errors and Tolerances

In an array with a number of antennas, the delays are adjusted relative to the delay for a designated reference antenna. We consider the reference antenna to be the one that is the last one encountered by the approaching wavefront, and its instrumental delay remains fixed. The delay error for any antenna is the difference between the sum of the geometric and instrumental delays for that antenna and for the reference antenna. When the delay error becomes as large as $\pm\tau_s/2$, the delay is adjusted by an increment $\pm\tau_s$. Thus, the delay error for a single antenna is uniformly distributed over $\pm\tau_s/2$. Coarse delay adjustments in units of the digital sampling interval are implemented in a FIFO (first-in-first-out) memory. These provide the major part of the instrumental delay, but the residual delay errors are large enough that they can cause serious loss of sensitivity if not mitigated. In the original VLA system, for example, finer steps were provided by an adjustment in the timing of the sampler action in steps of $\tau_0 = \tau_s/16$. The spacing of adjacent samples remains τ_s except when a delay adjustment is made and the sample occurs earlier or later by τ_0. When the delay error becomes equal to $\tau_0/2$, the instrumental delay is adjusted by τ_0, as represented by the staircase function in Fig. 7.10. One can see from Fig. 7.10 that the probability distribution of the delay error is uniform within a range $\pm\tau_0/2$. For a pair of antennas, it can usually be assumed that the times of delay adjustment are unrelated (in general, the rates of change of the geometric delay will be different for each antenna), so the probability distribution of their combined delay errors is a triangular function with extreme values of $\pm\tau_0$, as in Fig. 7.11. The rms value of this delay error is:

$$\left[\frac{\int_0^{\tau_0} p(\Delta\tau)\Delta\tau^2 d\Delta\tau}{\int_0^{\tau_0} p(\Delta\tau)\, d\Delta\tau}\right]^{1/2} = \frac{\tau_0}{\sqrt{6}}\,, \tag{7.42}$$

where $p(\Delta\tau)$ is the expression for the probability distribution of $\Delta\tau$ in Fig. 7.11.

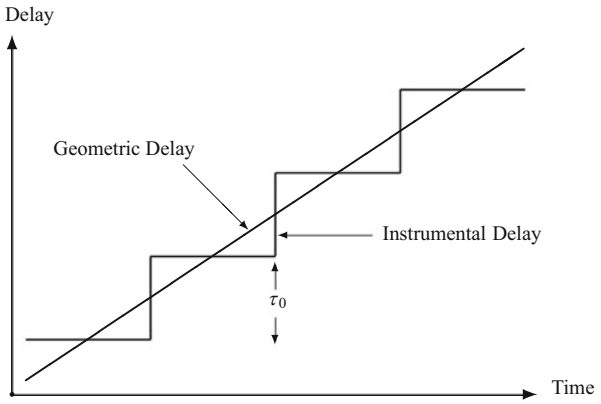

Fig. 7.10 Adjustment of instrumental delay in steps τ_0 to compensate for geometric delay. The vertical sections of the staircase function indicate change of instrumental delay, and the horizontal sections are the time intervals during which the signal is sampled. Over small time intervals, the geometric delay can be represented as a linear function of time. Both axes have the dimensions of time but, for example, a baseline of 1 km east–west, the maximum slope of the line representing space delay is 0.24 ns per second, and the timescales of the two axes differ by a factor of order 10^{10}.

7.3.6 Phase Errors and Degradation of Sensitivity

A delay error $\Delta\tau$ results in a phase error in a signal equal to $2\pi\Delta\tau\nu$ where, for systems using analog delays, ν represents the frequency in the IF band in which the delays are inserted. For systems in which the signal passband is Nyquist sampled, which is the most usual case, ν is a baseband frequency in the range 0 to $\Delta\nu$. With a spectral correlator, the highest frequency channel within such a band has a center frequency that is approximately equal to the high-frequency edge, $\Delta\nu$. For frequencies in this top channel, the maximum delay error τ_0 for an antenna pair results in a phase error of $2\pi\Delta\nu\tau_0 = (\tau_0/\tau_s)\pi$. Thus, the probability distribution of this phase error is a triangular function as in Fig. 7.11 with extreme values $\pm(\tau_0/\tau_s)\pi$. As shown for the delay error in Eq. (7.42), the rms phase error is the maximum value divided by $\sqrt{6}$.

To determine the effect of delay errors on sensitivity, note that for frequency ν, a delay error $\Delta\tau$ results in a phase error $2\pi\nu\Delta\tau$. Let α be the size of the fine step as a fraction of the coarse step τ_s. The sensitivity (i.e., the relative response) is determined by averaging the cosine of the phase error, weighted by the triangular distribution of delay error in Fig. 7.11,

$$\frac{2}{\alpha\tau_s}\int_0^{\alpha\tau_s}\left(1-\frac{\Delta\tau_s}{\alpha\tau_s}\right)\cos(2\pi\nu\Delta\tau)\,d\Delta\tau = \left[\frac{\sin(\pi\nu\alpha\tau_s)}{\pi\nu\alpha\tau_s}\right]^2 . \tag{7.43}$$

This is the sensitivity for a very small bandwidth centered on frequency ν, as in the case for spectral line observations. For continuum observations, the sensitivity for a band extending from $N\Delta\nu$ to $(N+1)\Delta\nu$, where N is any integer (including zero),

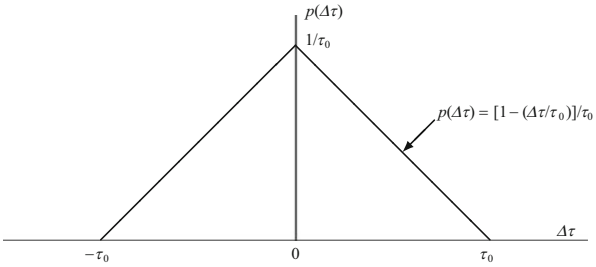

Fig. 7.11 Probability distribution $p(\Delta\tau)$ of the delay error $\Delta\tau$ for a pair of antennas. τ_0 is the minimum increment of the instrumental compensating delay. The expression shown for $p(\Delta\tau)$ applies to the part of the probability function for which $\Delta\tau \geq 0$.

is obtained by averaging over the baseband response,

$$\frac{1}{\Delta\nu}\int_0^{\Delta\nu\alpha\tau_s}\left[\frac{\sin(\pi\nu\alpha\tau_s)}{\pi\nu\alpha\tau_s}\right]^2 d\nu = \frac{2}{\alpha}\int_0^{\frac{\alpha}{2}}\left[\frac{\sin(\pi x)}{\pi x}\right]^2 dx\,. \tag{7.44}$$

Here, we use $\Delta\nu\tau_s = \frac{1}{2}$ and have put $\nu\alpha\tau_s = x$ for convenience in numerical evaluation of the integral.[3] For the case in which we use only the coarse delay steps ($\alpha = 1$), Eq. (7.44) is equal to 0.774, so, as noted earlier, the performance with coarse delay steps without further mitigation is not acceptable. Some values of rms phase error and sensitivity loss averaged across the bandwidth are given in Table 7.3.

In Table 7.3, sensitivity loss for $\alpha = 1/4$ is approaching an acceptable level. However, the maximum phase errors are $\sqrt{6} = 2.45$ times the rms value, i.e., $2.45\times 10.6° = 26°$ in this case. Depending upon how fast the delay error is changing with time, the maximum error will be decreased somewhat in the data averaging after cross-correlation. In the (u, v) plane, the rate of change of delay error goes through zero as the u-component of the baseline crosses the v axis. Thus, averaged data in which the phase error is close to the maximum are to be expected, especially for short-baseline configurations. Hence, in considering the acceptable delay errors, phase errors should be considered as well as sensitivity loss. The original VLA system used $\tau_s = 16\tau_0$ and a baseband IF response.

[3]In the case in which the phase errors are small, it may be convenient to use $\langle\cos(\phi)\rangle \approx (1 - \langle\phi^2\rangle/2)$, where $\phi = 2\pi\nu\alpha\Delta\tau$ and $\langle\,\rangle$ indicates the mean value. Then noting that $\Delta\tau$ and ν vary independently, $\langle\phi^2\rangle = (2\pi)^2\langle\Delta\tau^2\rangle\langle\nu^2\rangle$. From Eq. (7.42), $\langle\Delta\tau^2\rangle = \tau_0^2/6$, and for a baseband response, $\langle\nu^2\rangle = \Delta\nu^2/3$.

Table 7.3 Values of the loss in signal-to-noise ratio (sensitivity) for the full baseband response from 0 to $\Delta\nu$, as used in continuum observations

$\alpha = \tau_0/\tau_s$	$\phi_{\rm rms}$	SNR loss
1/4	10.6°	1.7%
1/8	5.30°	0.43%
1/16	2.65°	0.11%
1/32	1.33°	0.027%

7.3.7 *Other Methods of Mitigation of Delay Errors*

Conceptually, the most straightforward way of keeping the loss in sensitivity resulting from delay errors within a tolerable limit[4] (say, $\sim$ 1%) is to use a small enough value for the minimum delay increment. This may not always be easy in systems with wide bandwidths, which require correspondingly high sample rates in the digitization. A possible scheme to reduce phase errors (D'Addario 2003) is one in which whenever a delay increment is inserted or removed, a phase jump of magnitude $2\pi\nu_0\tau_0$, and opposite sign to the delay-induced phase jump, is inserted in the corresponding signal through an LO.[5] Here, ν_0 is the IF center frequency, for which the phase error is exactly canceled. The overall effect for the full bandwidth can be found by determining the value of $\langle(\nu-\nu_0)^2\rangle$, that is, the mean squared value of frequency measured with respect to the band center:

$$\langle(\nu-\nu_0)^2\rangle = \frac{1}{\Delta\nu}\int_{\nu_0-\Delta\nu/2}^{\nu_0+\Delta\nu/2}(\nu-\nu_0)^2\,d\nu = \frac{\Delta\nu^2}{12}\,. \tag{7.45}$$

This result applies to any IF band of width $\Delta\nu$. Since the phase changes resulting from the changes in the instrumental delay provide a component of the frequency offset used to stop the interferometer fringes, it is necessary to account for this effect by inserting a smooth component in the form of a frequency offset, $2\pi\nu_0\,d\tau_g/dt$, where τ_g is the geometric delay. This could be combined with the fringe-rotation offset in an LO.[6] The combination of the inserted phase jumps and the frequency

[4] Various effects in an interferometer system limit the sensitivity. There are some large effects, such as aperture efficiency and quantization efficiency, and more numerous smaller ones, such as phase irregularities in frequency responses, LO noise, timing errors, delay errors, etc. The combined effect of the smaller losses can become serious, so for each one, it is reasonable to aim at a fairly stringent limit such as the 1% figure suggested here.

[5] This method of mitigation of the delay errors was considered but not implemented during the early development of the VLA. The original idea is attributed to B. G. Clark.

[6] In the case of a double-sideband system, the fringe rotation must be applied to the first LO, but the frequency offset required by the phase error reduction scheme must be applied to the second or a later LO so that, like the delay-induced phase errors, the offsets are applied with the same sign to each sideband component within the IF band.

offset provides a sawtooth phase component that, at the band center, exactly cancels the phase sawtooth induced by the delay error. If this method were used with no fine delay steps, i.e., $\tau_0 = \tau_s$, the loss in sensitivity would be $\sim 13\%$, so a combination with some finer steps would be necessary.

7.3.8 Multichannel (Spectral Line) Correlator Systems

In multichannel correlators, the input band is divided into many channels, and the signals for corresponding channels are cross-correlated. The number of channels is usually an integral power of two and commonly 1024 or more. Within any channel, the relative variation of frequency is very small. Thus, at any instant, the effect of a delay error $\Delta\tau$ is to introduce a phase error $2\pi\Delta\tau\nu_c$, where ν_c is the center frequency of the channel. Since the frequency variation is small across a single channel, the loss in signal amplitude that occurs in a wide (continuum) band, resulting from the frequency variation of the phase error, is avoided. The time variation of the delay error results in a varying phase error that can be corrected by inserting a phase correction for each channel at the correlator. Thus, with a multichannel correlator, it is possible to avoid the need for delay increments finer than τ_s, so long as the extra processing steps to correct the phase can be incorporated. For an individual antenna, the maximum delay error is $\tau_s/2 = 1/(2\Delta\nu)$, and for the highest channel, centered very close to frequency $\Delta\nu$, the maximum phase error is π. The time for the delay error variation to complete one cycle is $\frac{d\tau}{dt}/\tau_s = \frac{d\tau}{dt}\Delta\nu/2$. (Note that the rate of change of delay, $\frac{d\tau}{dt}$, is different for each antenna.) This is greater than the time for one fringe cycle by a factor of $2 \times$ (signal frequency at the antenna)/(signal frequency in the baseband $0 - \Delta\nu$). At any instant, the phase error for the signal from an antenna is equal to $2\pi \times$ (delay error) $\times$ (channel frequency in the baseband $0 - \Delta\nu$). If the correction is applied at the correlator output, the corrections for both antennas of each pair must be included.

Carlson and Dewdney (2000) describe a multichannel correlator designed to handle wide bandwidth signals (the WIDAR system). The signals from the antennas are Nyquist sampled, and then the band is divided into a number of channels, N_c. The Nyquist sample rate appropriate for each channel is equal to the original sample rate divided by N_c, and the sample rates are adjusted to this value at the filter outputs. The outputs of the filters then go to separate cross-correlators. In this way, the total bandwidth that can be processed is not limited by the capacity of a single correlator. A value of $N_c = 32$ would be sufficient to reduce the loss in sensitivity resulting from the delay errors to an acceptably small value. Adjusting the phases of the signals at the correlator inputs removes the phase errors resulting from delay errors and also provides fringe stopping. Phase adjustment at this point is possible because the samples are in complex form, having been through the filtering process. Since multichannel correlators give a means of removing channels that are contaminated by interference, they are widely used for continuum as well as spectral line observations.

7.3.9 Double-Sideband Systems

The considerations up to this point have applied to single-sideband (SSB) systems. For double-sideband (DSB) systems, some differences must be considered (Thompson and D'Addario 2000). For an SSB system, the main effect of a phase error is to cause a rotation of the correlation vector, as indicated in Fig. 6.5a, resulting in an error in the correlator output phase, as considered above.[7] For a DSB system, the delay error causes the components of the correlation vector resulting from the two sidebands to rotate in opposite directions in the complex plane, as shown in Fig. 6.5b, where the line *AB* represents the phase angle when the delay error is zero.[8] The amplitude of the vector sum of the two components is proportional to $\cos(2\pi\nu_0\Delta\tau)$, where ν_0 is the IF center frequency, but the phase of the correlation is not changed by a variation in the instrumental delay.

Consider a case in which the geometric delay is varying rapidly enough that the delay error changes sign several times during the minimum averaging time at the correlator output. For an SSB system (Fig. 6.5a), the phase of the correlation vector swings back and forth, following the difference of the error patterns for the two antennas (the small arrows indicating variation of the vector phase in Fig. 6.5 reverse direction when the sign of the phase error changes). For a DSB system (Fig. 6.5b), the phase angles of the vectors representing the two sideband responses move in opposite senses. In both the SSB and DSB cases, components of the correlation that are normal to the vector time-average (in Fig. 6.5b, the line *AB*) cancel, and the magnitude of the correlation is proportional to the time average of the cosine of the phase measured with respect to the mean phase. Over an averaging period in which the SSB phase error changes sign, the loss in sensitivity is effectively the same for the SSB and DSB systems. Note, however, that in the SSB case, the loss in sensitivity occurs in the averaging, whereas in the DSB case, the loss occurs immediately in the correlation process. Thus, in the SSB case, there is an opportunity to correct for phase errors after cross-correlation, but in the DSB case, this is possible only if the sideband responses can be separated.

If we are considering delay errors that are quasi-constant, or vary only slowly with time, the tolerance on the errors is more stringent in the DSB case. Such errors were more important in early interferometers with analog delay systems using coaxial cable or ultrasonic elements (see, e.g., Coe 1973), which could be temperature sensitive and difficult to calibrate accurately. In digital systems, the delays are controlled by a highly accurate master clock, and the only significant

[7] There is also a relatively small decrease in the amplitude, which results from the variation of the phase error with frequency across the IF band and is proportional to $\mathrm{sinc}(\Delta\nu\Delta\tau)$, where $\Delta\nu$ is the IF bandwidth. This results from the averaging of the varying phase over time. The same sinc function appears as part of Eq. (6.9) and is shown by the broken line in Fig. 6.4.

[8] To measure the phase of the cross-correlation of both sidebands in combination, it is necessary to periodically insert a $\pi/2$ phase shift into the IF signal of one antenna, or not to stop the fringes and fit a sine wave to the fringe function.

errors result from the incremental nature of the adjustment. With digital delays, the effects are in most respects the same for SSB and DSB systems, except that for DSB systems, again, post-correlation corrections are possible only if the sidebands can be separated.

In addition to causing a loss in sensitivity, delay-induced phase errors contribute to errors in the phase of the measured visibility. In this case, the values after time averaging, not the instantaneous values, are critical. The effective averaging time is of the order of the time taken for the baseline vector to cross a cell in the simple case of cell averaging, discussed in Sect. 5.2.2. In a synthesis array, the compensating delay for each antenna is adjusted to equalize the delay relative to some celestial reference point as the source moves across the sky. If the antenna spacings are large, the delay may change by several increments during most cell crossings, and the resulting phase errors are reduced by the data averaging. However, for any pair of antennas, the rate of change of the geometric delay, which is proportional to u, goes through zero when the baseline vector crosses the v axis.

In conclusion, the tolerances in Table 7.2 apply to the overall system from the antennas to the correlator inputs. Specifications of filters that define the passband should include consideration of the temperature effects discussed in Sect. 7.2.7. The frequency selectivity of elements in the earlier stages can then be held to the minimum required for rejection of interfering signals. There are advantages to implementing the filtering that defines the passband digitally, after the sampling, instead of in the analog stages [see, e.g., Prabu et al. (2015)].

7.4 Polarization Mismatch Errors

The response of two antennas to an unpolarized source is greatest when the antennas are identically polarized. Small variations in the polarization characteristics of one antenna relative to another occur as a result of mechanical tolerances. These variations lead to errors in the assignment of antenna gains in a manner similar to the variations in frequency responses. To examine this effect, we calculate the response of two arbitrarily polarized antennas to a randomly polarized source, which is given by the term for the Stokes parameter I_v in Eq. (4.29). Definitions of symbols are in terms of the polarization ellipse (see Fig. 4.8 and related text). The position angle of the major axis is ψ, the axial ratio is $\tan\chi$, and subscripts m and n indicate two antennas of an array. As an example, we consider antennas with nominally identical circular polarization for which we can write $\chi_m = \pi/4 + \Delta\chi_m$ and $\chi_n = \pi/4 + \Delta\chi_n$, where the Δ terms represent the deviations of the corresponding parameter from the ideal value. The required response is

$$G_{mn} = G_0 \left[\cos(\psi_m - \psi_n)\cos(\Delta\chi_m - \Delta\chi_n) + j\sin(\psi_m - \psi_n)\cos(\Delta\chi_m + \Delta\chi_n)\right] . \tag{7.46}$$

Now $\psi_m - \psi_n$ and the Δ terms represent construction tolerances and are all small. Thus, we can expand the trigonometric functions and retain only the first- and second-order terms. Equation (7.46) then becomes

$$G_{mn} = G_0 \left\{ 1 - \frac{1}{2} \left[(\psi_m - \psi_n)^2 + (\Delta\chi_m - \Delta\chi_n)^2 \right] + j(\psi_m - \psi_n) \right\} . \qquad (7.47)$$

An analysis similar to the procedure for frequency responses in Sect. 7.3 can be made by assigning polarization characteristics to a model group of antennas and determining pair gains, best-fit antenna gains, and gain residuals. For simplicity, it is assumed that the spread of values is of similar magnitude for the parameters χ and ψ. A 1% maximum gain residual then results from a spread of $\pm 3.6°$ in χ and ψ. A value of $\Delta\chi = 3.6°$ corresponds to an axial ratio of 1.13 for the polarization ellipse, and it is not difficult to obtain feeds for which the deviation from circularity is within this value near the beam center. A similar analysis for linearly polarized antennas gives tolerances of the same order (Thompson 1984).

7.5 Phase Switching

7.5.1 Reduction of Response to Spurious Signals

The technique of phase switching for a two-element interferometer has been described in Chap. 1, where it was explained as an early method of obtaining analog multiplication of signals. The principle is as indicated in Fig. 1.8. However, in later instruments, the power-law detector is replaced by a correlator. Although more direct methods of signal multiplication are now used, phase switching is still useful to eliminate small offsets in correlator outputs that can result from imperfections in circuit operation or from spurious signals. The latter are difficult to eliminate entirely in any complicated receiving system, since combinations of harmonics of oscillator frequencies that fall within the observing frequency band or any IF band may infiltrate the electronics. Such signals, at levels too low to detect by simple test procedures, can be strong enough to produce unwanted components in the output. For an array of n_a antennas, a receiving bandwidth $\Delta\nu$, and an observing duration τ, signals at the limit of detectability are at a power level of order $(n_a\sqrt{\Delta\nu\tau})^{-1}$ relative to the noise; for example, this gives 75 dB below the noise for $n_a = 27$, $\Delta\nu = 50$ MHz, and $\tau = 8$ h. Similar effects can also be produced by cross coupling of small amounts of noise from one IF system to another. Because such spurious signals produce components of the visibility that change only slowly with time, they show up as spurious detail near the origin of the image. If they enter the signal channel at a point that comes after the phase switch, so that they produce a component with no switch-frequency variation at the synchronous detector, they can generally be reduced by several orders of magnitude by the phase switching.

7.5.2 Implementation of Phase Switching

Consider the problem of phase switching in a multielement array in which the products of the signals from all possible pairs of antennas are formed. Phase switching can be represented by multiplication of the received signals by periodic functions that alternate in time between values of +1 and −1. For the mth and nth antennas, let these functions be $f_m(t)$ and $f_n(t)$. Synchronous detection of the correlator output for these two antennas requires a reference waveform $f_m(t)f_n(t)$, and any nonvarying, unswitched components from the multiplier are reduced by a factor

$$\frac{1}{\tau}\int_0^{\tau} f_m(t)f_n(t)\,dt \tag{7.48}$$

after averaging for a time τ. For the periodic waveforms that we are concerned with, this factor will be zero if τ is a multiple of the minimum period of orthogonality τ_{or} for $f_m(t)$ and $f_n(t)$. In fact, unwanted output components may not be exactly constant, because the tracking of the compensating delays introduces slow changes in the phases with which the spurious signals are combined. However, the unwanted outputs will be strongly reduced by the synchronous detection as long as their variation is small over the period τ_{or}. If the orthogonality of the phase-switching functions depends on the relative timing of transitions, the timing should be adjusted so that the functions are orthogonal at the correlator inputs. Thus, it may be necessary to adjust the timing of the switching waveforms at the antennas to compensate for the varying instrumental delays inserted as a source moves across the sky.

Implementation of phase switching on an array of n_a antennas calls for n_a mutually orthogonal, two-state waveforms. Square waves whose frequencies are proportional to integral powers of two are orthogonal, with τ_{or} equal to the period of the lowest nonzero frequency.[9] In phase switching, τ_{or} is equal to the data averaging time, which is typically a few seconds but for special cases may be as low as 10 ms. The shortest interval between switching transitions τ_{sw} is equal to the half-period of the fastest square wave. Technically, it is convenient if $\tau_{\text{or}}/\tau_{\text{sw}}$ does not greatly exceed about two orders of magnitude. If one antenna remains unswitched, then $\tau_{\text{or}}/\tau_{\text{sw}} = 2^{n_a-1}$. Square waves of the *same* frequency are orthogonal if their phases differ by a quarter of a cycle in time. When this condition for orthogonality is also included, $\tau_{\text{or}}/\tau_{\text{sw}} = 2^{n+1}$, where n is the smallest integer greater than or equal to $(n_a - 3)/2$. This reduces the value of $\tau_{\text{or}}/\tau_{\text{sw}}$, but the orthogonality then depends upon the relative timing of the transitions at the correlator, which is not the case for square waves of different frequencies. In either case, $\tau_{\text{or}}/\tau_{\text{sw}}$ is inconveniently large for a large array and, for example, for $n_a = 27$, it is of order 10^8 in the first case and 10^4 in the second.

[9] Such waveforms are sometimes referred to as Rademacher functions.

It is useful to note that a condition for a pair of square waves of different frequency to be orthogonal, for arbitrary time shifts, is that they do not contain Fourier components of the same frequency. A property of square waves is that all even-numbered Fourier components (i.e., even harmonics of the fundamental frequency) have zero coefficients, but odd-numbered components have nonzero coefficients. Thus, although sinusoids with frequencies proportional to 1, 2, 3, ... are mutually orthogonal, square waves with such frequencies, in general, are not. For example, square waves of frequencies 1, 2, and 4 have no common Fourier components and are mutually orthogonal, but 1, 3, and 5 have common components and are not mutually orthogonal. D'Addario (2001) shows by generalization of this analysis that the lowest frequency sets of N mutually orthogonal square waves consist of those with frequencies proportional to 2^n for $n = 0,\ 1, \ldots, (N-1)$, that is, the square-wave sets discussed above. Since the different square waves of a set that we are considering contain no common Fourier components, their orthogonality is not affected by relative time shifts. Note, also, that exact orthogonality is not essential for phase switching. Unwanted responses can be reduced by a factor of 10^4 or more by using square waves with k cycles per averaging period for values of k that are prime numbers greater than 100.

For arrays with large numbers of antennas, Walsh functions are generally the preferred waveforms for phase switching. Walsh functions are rectangular waveforms in which transitions between $+1$ and -1 occur at intervals that are a varying integral submultiple of a basic time cycle, as in Fig. 7.12. For a description of Walsh functions (Walsh 1923; also Fowle 1904) see, for example, Harmuth (1969, 1972) or Beauchamp (1975). Various systems of designating and ordering Walsh functions are in use. In one system (Harmuth 1972), those with even symmetry are designated as cal(k, t) and those with odd symmetry as sal(k, t). Here, t is time expressed as a fraction of the time base T, which is the interval at which the waveform repeats, and k is the *sequency*, which is equal to half the number

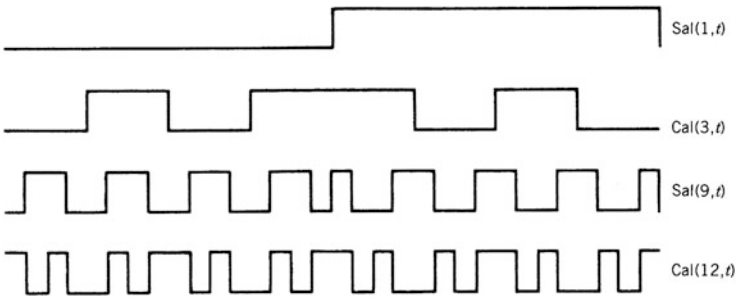

Fig. 7.12 Four examples of Walsh functions, each of which repeats after the one cycle of the time base interval plotted above. Within this interval, the sal functions are odd, and the cal functions are even. The value of each function alternates between 1 and -1. The first number in parentheses in the name of each function is the sequency, which is equal to half the number of zero crossings in the time base interval. Time t is measured as a fraction of the time base.

of zero crossings within the time base. Walsh functions with different sequencies are orthogonal, and cal and sal functions of the same sequency are orthogonal but differ only by a time offset. The orthogonality requires that the time bases of the individual Walsh functions be aligned in time, so time offsets are not permitted. Walsh functions with sequencies that are integral powers of two are square waves. If one antenna is unswitched, and if only the cal or only the sal functions are used, the highest sequency required is $n_a - 1$. Then $\tau_{\text{or}}/\tau_{\text{sw}} = 2n$, where n is the smallest power-of-two integer greater than or equal to $n_a - 1$. If both cal and sal functions are used, then n is the smallest power-of-two integer greater than or equal to $(n_a - 1)/2$. For example, for $n_a = 64$, $\tau_{\text{or}}/\tau_{\text{sw}}$ is 128 in the first case and 64 in the second. Another designation for Walsh functions, wal(n, t), includes both cal and sal functions, cal(n, t) = wal$(2n, t)$ and sal(n, t) = wal$(2n - 1, t)$.

One method of generating Walsh functions makes use of Hadamard matrices, of which the one of lowest order is

$$H_2 = \begin{bmatrix} 1 & 1 \\ 1 & -1 \end{bmatrix} . \tag{7.49}$$

Higher-order Hadamard matrices can be obtained by replacing each element of H_2 by the matrix H_2 multiplied by the element replaced [which is equivalent to forming an outer product; see Eq. (4.48)]. If this is performed twice, for example, we obtain

$$H_8 = \begin{bmatrix} 1 & 1 & 1 & 1 & 1 & 1 & 1 & 1 \\ 1 & -1 & 1 & -1 & 1 & -1 & 1 & -1 \\ 1 & 1 & -1 & -1 & 1 & 1 & -1 & -1 \\ 1 & -1 & -1 & 1 & 1 & -1 & -1 & 1 \\ 1 & 1 & 1 & 1 & -1 & -1 & -1 & -1 \\ 1 & -1 & 1 & -1 & -1 & 1 & -1 & 1 \\ 1 & 1 & -1 & -1 & -1 & -1 & 1 & 1 \\ 1 & -1 & -1 & 1 & -1 & 1 & 1 & -1 \end{bmatrix} \begin{matrix} \text{cal}(0, t), \ \text{pal}(0, t) \\ \text{sal}(4, t), \ \text{pal}(4, t) \\ \text{sal}(2, t), \ \text{pal}(2, t) \\ \text{cal}(2, t), \ \text{pal}(6, t) \\ \text{sal}(1, t), \ \text{pal}(1, t) \\ \text{cal}(3, t), \ \text{pal}(5, t) \\ \text{cal}(1, t), \ \text{pal}(3, t) \\ \text{sal}(3, t), \ \text{pal}(7, t) \ . \end{matrix} \tag{7.50}$$

The rows of the matrices correspond to the Walsh functions indicated, the signs being reversed for odd sequencies in this particular generation process. The waveform required at the phase detector is the product of the phase-switching functions at the two antennas involved. The product of two such Walsh functions is a Walsh function, the sequency of which is greater than, or equal to, the difference between the sequencies of the two original functions.

Walsh functions can also be generated as products of square-wave functions. Square-wave functions are here designated Sq(n, t), where n is an integer and the half-period of the square wave is $T/2^n$; that is, there are 2^{n-1} complete cycles within the time base, T. The function Sq$(0, t)$ has a constant value of unity. In the examples in Fig. 7.12, sal$(1, t)$ is a square-wave function, and cal$(3, t)$ and sal$(9, t)$ are each products of sal$(1, t)$ and one other square-wave function. When considering Walsh functions as products of square-wave functions, it is convenient to use the Paley

designation of Walsh functions, pal(n, t) (Paley 1932). The integer n is called the *natural order* of the Walsh function. A Walsh function pal(n, t), which is the product of square-wave functions Sq(i, t), Sq(j, t), ..., Sq(m, t), has a natural order number $n = 2^{i-1} + 2^{j-1} +, \ldots, +2^{m-1}$. The product of two Walsh functions is another Walsh function, of which the natural order number is given by modulo-2 addition (that is, no-carry addition) of the binary natural order numbers of the component Walsh functions.

Table 7.4 shows the relationship between the natural order numbers for a series of Walsh functions and the square-wave functions of which they are composed. The product of two Walsh functions can be expressed as the product of the component square-wave functions, for example,

$$\begin{aligned} \text{pal}(7, t) \times \text{pal}(10, t) &= [\text{Sq}(1, t) \times \text{Sq}(2, t) \times \text{Sq}(3, t)] \times [\text{Sq}(2, t) \times \text{Sq}(4, t)] \\ &= \text{Sq}(1, t) \times \text{Sq}(2, t) \times \text{Sq}(2, t) \times \text{Sq}(3, t) \times \text{Sq}(4, t) \\ &= \text{Sq}(1, t) \times \text{Sq}(3, t) \times \text{Sq}(4, t) \\ &= \text{pal}(13, t) \ , \end{aligned} \tag{7.51}$$

where we have used the fact that the product of a Walsh or square-wave function with itself is equal to unity. The natural orders of the two Walsh functions, 7 and 10, in binary form are 0111 and 1010. The modulo-2 addition of these binary numbers is 1101, which is equal to 13, the natural order of the Walsh function product.

Table 7.4 Square-wave components of some Walsh functions

Natural order designation	Square-wave components					Sequency designation
	Sq$(0, t)$	Sq$(1, t)$	Sq$(2, t)$	Sq$(3, t)$	Sq$(4, t)$	
pal(0,t)	1					cal(0,t)
pal(1,t)		1				sal(1,t)
pal(2,t)			1			sal(2,t)
pal(3,t)		1	1			cal(1,t)
pal(4,t)				1		sal(4,t)
pal(5,t)		1		1		cal(3,t)
pal(6,t)			1	1		cal(2,t)
pal(7,t)		1	1	1		sal(3,t)
pal(8,t)					1	sal(8,t)
pal(9,t)		1			1	cal(7,t)
pal(10,t)			1		1	cal(6,t)
pal(11,t)		1	1		1	sal(7,t)
pal(12,t)				1	1	cal(4,t)
pal(13,t)		1		1	1	sal(5,t)
pal(14,t)			1	1	1	sal(6,t)
pal(15,t)		1	1	1	1	cal(5,t)

The examination of Walsh functions as products of square-wave functions leads to a useful insight into the efficiency of Walsh function phase switching in eliminating unwanted components (Emerson 1983, 2009). Let $\mathcal{U}(t)$ be an unwanted response within the receiving system, for example, resulting from cross talk in IF signals or from an error in the sampling level of a digitizer. $\mathcal{U}(t)$ arises after the initial phase switching, so when synchronous detection with the phase-switching waveform is performed at a later stage, $\mathcal{U}(t)$ becomes $\mathcal{U}(t)\text{pal}(n,t)$, and this product is significantly reduced in the subsequent averaging. Suppose that $\text{pal}(n,t)$ is the product of m square-wave functions, $\text{Sq}(1,t), \text{Sq}(2,t), \ldots, \text{Sq}(m,t)$. We can consider multiplying $\mathcal{U}(t)$ by $\text{pal}(n,t)$ as equivalent to multiplying by each of the square-wave components in turn. Also, we assume that the period of the square-wave functions is small compared with the timescale of variations of $\mathcal{U}(t)$. Then, after the first multiplication and averaging, the mean residual spurious voltage is

$$\mathcal{U}_1(t) = \frac{[\mathcal{U}(t) + \delta t \frac{d\mathcal{U}}{dt}] - \mathcal{U}(t)}{2} = \frac{\delta t}{2}\frac{d\mathcal{U}}{dt} = \frac{T}{2^{i+1}}\frac{d\mathcal{U}}{dt}\,, \tag{7.52}$$

where δt is equal to the half-period of the square-wave function, $T/2^i$. $\mathcal{U}_1$ is calculated for one cycle of $\text{Sq}(i,t)$, but within the assumption that $\mathcal{U}(t)$ is slowly varying, $\mathcal{U}_1$ can be taken as equal to the average over the Walsh time base T. Multiplication by the second square-wave function is obtained by replacing $\mathcal{U}$ in Eq. (7.52) by $\mathcal{U}_1$, which yields

$$\mathcal{U}_2(t) = \frac{T}{2^{j+1}}\frac{d\mathcal{U}_1}{dt} = \frac{T^2}{2^{i+j+2}}\frac{d^2\mathcal{U}}{dt^2}\,. \tag{7.53}$$

For the m square-wave components, we obtain

$$\mathcal{U}_m(t) = \frac{T^m}{2^{(1+2+\cdots+m)}}\frac{d^m\mathcal{U}}{dt^m}\,, \tag{7.54}$$

so only the higher derivatives of $\mathcal{U}$ remain.

Walsh functions $\text{pal}(n,t)$ for which n is an integral power of two are the least effective in eliminating unwanted responses, since they are each just a single square-wave function. As shown by examination of Table 7.4, those for which $n = 2^k - 1$, where k is an integer, contain the largest number of square-wave components. In arrays with a small number of antennas, for which a large number of different switching functions is not required, it is possible to select Walsh functions that are the most effective in reducing unwanted components. Similarly, Walsh functions can be more effective than square waves in some applications to single antennas, such as beam switching between a source and a reference position on the sky (Emerson 1983). Another set of possible phase-switching functions are m-sequences, considered by Keto (2000) for cases in which both 90° and 180° phase changes are required.

7.5.3 *Timing Accuracy in Phase Switching*

In designing a phase-switching system, timing tolerances should be considered. In general, the accuracy should be much smaller than the minimum interval between transitions in any function. For example, in ALMA [the Atacama Large Millimeter/submillimeter Array, Wootten (2003), Wootten and Thompson (2009)], two phase-switching actions are used, one nested within the other (Emerson 2007). For sideband separation, $\frac{\pi}{2}$ phase-switching is used, with Walsh functions from a 128-element set with time base 2.048 s and minimum interval between transitions of 16 ms. A second 128-element set with time base 16 ms and minimum interval 125 μs is used for π-shift switching. Thus, timing errors must be very small compared with 125 μs.

In general, the orthogonality of Walsh functions requires that there be no relative time shifts between the functions. The first switching occurs at the antenna location, that is, as early in the signal path as possible. Digitization of the received signal may occur at the antenna or after transmission of the signal in analog form to a central processing location. The major system delays are shown in Fig. 7.13, in which τ_g is the geometric delay, τ_{tr} is the transmission delay (antenna to processing location), and τ_i is the instrumental compensating delay. Delays in the analog or digital circuitry are generally small enough to be neglected with regard to the timing of phase switching. There are three main timing requirements in the receiving system.

1. The total delay from the incident wavefront to the correlator input, $\tau_g + \tau_{\text{tr}} + \tau_i$, must be the same for all antennas to preserve the correlation of the wanted signals. This is implemented through adjustment of τ_i.
2. The corresponding transitions in the first and second phase switchings should be aligned in time so that the phase switching of the wanted signals is precisely

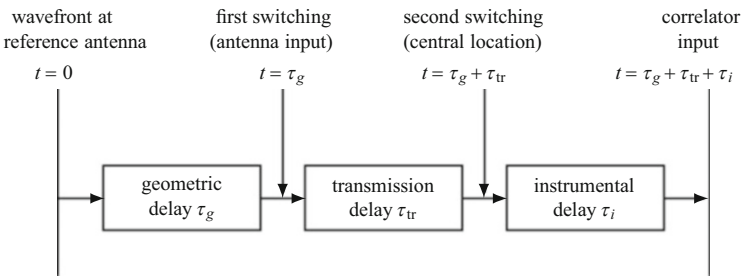

Fig. 7.13 Delays in an array that are large enough to affect the timing of the Walsh functions used in phase switching. Here, t is time relative to a signal wavefront at the point where it intercepts the delay reference antenna. The second switching is shown after the transmission delay, which applies when the signals are transmitted in analog form to the central processing location. When digitization occurs at the antenna location, both the first and second switchings can be applied before the transmission delay.

canceled. For example, if the second phase switching is done at the central location, the timing of the second switching should be delayed relative to the first one by τ_{tr}.

3. Both the first and second switchings in any signal path should be delayed by the geometric delay of the corresponding antenna τ_g so that, at the correlator input, the switching transitions in the unwanted components are aligned in time from one antenna to another. The delay τ_g varies with time as the antennas track a source.

Requirement 2 above is concerned only with the relative accuracy of switchings within the same signal path from one antenna to the correlator. This is the simplest case because it is concerned only with offsets in two switchings of the same Walsh function. Consider the effect of a small time offset δ in the relative timing of the first and second switchings. For each transition, the timing difference causes the correlator output voltage to be reversed for a period δ and thereby cancels an equivalent interval of the unreversed output. Hence, for each transition, there is an effective loss of signal for a period 2δ. The average fractional loss of sensitivity is $2n_t\delta/\tau_{tb}$, where n_t is the number of transitions within the time base τ_{tb} (i.e., twice the Walsh sequency). Thus, for a tolerable limit of, e.g., 1% correlation loss, the tolerable value of δ can be determined for any given time base and maximum sequency used. Since the correlation loss is proportional to n_t, use of the lowest sequencies within the Walsh set helps to minimize loss in sensitivity. For arrays in which the numbers of antennas and the baseline lengths are not too long, the delaying of the switchings by τ_g (as noted in the third requirement above) can often be neglected. This introduces a timing error τ_g that is greatest for the longest baselines. The effect of this error can be minimized by using the lowest values of n_t for the antennas for which the geometric delay is greatest.

Requirements 1 and 3 are concerned with the relative timing of transitions at different antennas, i.e., between different Walsh functions. The effect of a timing offset on the rejection of the unwanted components depends on the loss in orthogonality of the Walsh functions used for different antennas. This is more complicated than the effect of an offset on two identical Walsh functions discussed above. The loss in orthogonality depends upon the sequencies of the two functions involved and is greatest for sequencies in the middle range of the Walsh set, as shown by Emerson (2005). Pairs consisting of a function with an even sequency and one with an odd sequency remain orthogonal in the presence of time shifts, but such combinations are possible for no more than half of the pairs in a complete Walsh set. Of the other pairs, some remain orthogonal with time offsets, as can be shown by numerical trials, and some do not [as shown in Fig. 3 of Emerson (2005)]. It is clearly beneficial to use equal numbers of odd and even sequencies in an array so that for approximately half of the antenna pairs, the orthogonality is independent of time offsets.

7.5.4 *Interaction of Phase Switching with Fringe Rotation and Delay Adjustment*

The effectiveness of phase switching in reducing the response to spurious signals depends on the point in the signal channel at which these unwanted signals are introduced. The three following cases illustrate the most important possibilities.

1. The unwanted signal enters the antennas or some point in the signal channels that is ahead of the phase switching, the fringe rotation, and the compensating delays. The unwanted signal then suffers phase switching like the wanted signals and is not suppressed in the synchronous detection (although it may be reduced by the fringe rotation if the fringe frequency is high, as in the case of VLBI). Externally generated interference behaves in this manner, and its effect is discussed in Chap. 16.
2. The unwanted signal enters after the phase switching but before the fringe rotation and delay compensation. The fringe-rotation phase shifts, designed to reduce to zero the fringe frequencies of the desired signals at the correlator output, act on the spurious signal and cause it to appear at the correlator output as a component at the natural fringe frequency for a point source at the phase reference position. This component then undergoes synchronous detection with a Walsh function. If the natural fringe frequency transiently matches the frequency of a Fourier component of this Walsh function, a spurious response can occur.
3. The spurious signal enters after the phase switching and the fringe rotation but before the delay compensation. The signal then suffers phase shifts resulting from the changing of the compensating delay. The resulting component at the correlator output has a frequency equal to the natural fringe frequency that would occur if the observing frequency were equal to the IF at which the compensating delays are introduced. Thus, the oscillations are one to three orders of magnitude lower in frequency than the natural fringe frequency, and it is consequently easier to avoid coincidence with the frequency of a component of the Walsh function.

From these considerations, it is usually advantageous to perform both the phase switching and the fringe rotation as early in the signal channel as possible. Figure 7.14 shows, as an example, the phase-switching scheme that was used in the original VLA system, from a description by Granlund et al. (1978). The phase switching at the antenna was performed on an LO, rather than on the full signal band, so that a broadband phase switch was not needed. The signals were digitized at the output of the final IF amplifier and thereafter were delayed and multiplied digitally. In such a system, slow phase drifts that may occur after the phase switching are removed by the synchronous detection at the digitizing sampler. The synchronous detection could be performed by reversing the sign bit in the digitized signal data and needed to be applied only to n_a signal channels rather than $n_a(n_a - 1)/2$ correlator outputs.

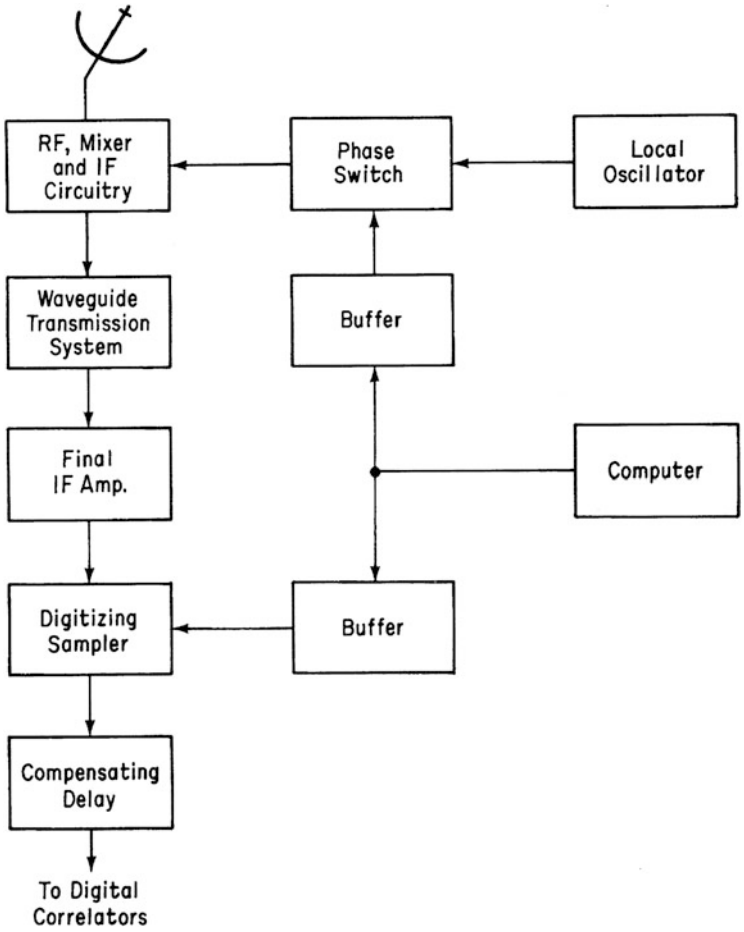

Fig. 7.14 Simplified schematic diagram of the receiving channel for one antenna of the original VLA system. Walsh functions generated by the computer were periodically fed to digital buffers, from which they were clocked out to the phase switch and to sign-reversal circuitry at the digitizing sampler. © 1978 IEEE. Reprinted, with permission, from J. Granlund et al. (1978).

7.6 Automatic Level Control and Gain Calibration

In most synthesis arrays, automatic level control (ALC) circuits are used to hold constant the level of the total signal, that is, the cosmic signal plus the system noise, at certain critical points. A fraction of the total signal level is detected, and the resulting voltage is compared with a preset value to generate a control signal that is fed back to a variable-gain element of the signal chain. Points at which the signal level is critical include modulators for transmission of IF signals on optical

or microwave carriers and inputs to analog correlators or digital samplers. For a discussion of level tolerances in samplers, see Sect. 8.5.1.

The effect of an ALC loop is to hold constant the quantity $|g|^2(T_S + T_A)\Delta\nu$, where g is the voltage gain from the antenna output to the point of gain control, T_S is the system temperature, and T_A is the component of antenna temperature due to the source under observation. Thus, $|g|^2$ is made to vary inversely as $(T_S + T_A)$, which can change substantially with the antenna pointing angle as a result of ground radiation in the sidelobes and atmospheric attenuation. To measure such gain changes, a signal from a broadband noise source can be injected at the input of the receiving electronics. This noise source is switched on and off, usually at a frequency of a few hertz to a few hundred hertz, and the resulting component is sampled and monitored using a synchronous detector. When the noise source is on, it adds a calibrating component T_C to the overall system temperature, which should not be more than a few percent of T_S to avoid degradation of sensitivity. The amplitude of the switched component is a direct measure of the system gain, and for $T_A \ll T_S$, the ratio of the signal levels with the noise source on and off is equal to $1 + T_C/T_S$, which provides a continuous measure of T_S. This scheme does not correct for changes in antenna gain resulting from mechanical deformation, which must be calibrated separately by periodic observation of a radio source.

7.7 Fringe Rotation

The fringe oscillations in the data from the correlator must be removed before an image can be formed. This process is sometimes referred to as fringe stopping (i.e., stopping the motion of the fringes with respect to the astronomical sky). As described in Chap. 6, this can be achieved by inserting a fringe-frequency offset on an LO. For a multiantenna array, the offset for each antenna is chosen to stop the fringes for that antenna when combined with a common reference antenna. It is also possible to stop the fringes by inserting corrections in the phase of the signals at the correlator. If the corrections are inserted before the cross multiplication that occurs in the correlation, they can be applied to each of the n_a antennas of the array (see, e.g., Carlson and Dewdney 2000), whereas after cross multiplication, the corrections must be applied to all of the $n_a^2/2$ antenna pairs. However, corrections inserted before cross multiplication must be applied to each signal sample that goes to the cross-correlator, whereas corrections applied to the cross products can be performed after some time-limited averaging of the products. (The averaging must not be so long that the fringe oscillations are attenuated.) The effect of time averaging on the fringes is to convolve the sinusoidal fringe function of frequency ν_f with a rectangular function of width equal to the averaging time τ_{av}. A 1% loss in sensitivity occurs for $\nu_f\tau_{\text{av}} = 0.078$ and 2% loss for $\nu_f\tau_{\text{av}} = 0.111$. As an approximate criterion, the averaging time should be no more than $\sim 1/10$ of a fringe

period. For a DSB system, the LO offset must be applied to the first LO, or if the fringe stopping is applied at the correlator, the sidebands must first be separated. For sideband separation, see Sect. 6.1.12.

Appendix 7.1 Sideband-Separating Mixers

The principle of the sideband-separating mixer, or image-rejection mixer, is shown in Fig. A7.1. The terms $\cos(2\pi\nu_u t)$ and $\cos(2\pi\nu_\ell t)$ represent frequency components of the input waveform at the upper- and lower-sideband frequencies, respectively. The input is applied to two mixers, for which the LO waveforms at frequency ν_{LO} are in phase quadrature. The mixers generate products of the signal and LO waveforms, and the filters pass only the terms of frequency equal to the difference of ν_{LO} and ν_u or ν_ℓ. The output from the lower mixer also passes through a $\pi/2$ phase lag network. From the resulting terms at points A and B, one can see that by applying the waveforms at these points to a summing network, the upper-sideband response is obtained. Similarly, by using a differencing network, the lower-sideband response is obtained. In either case, the accuracy of the suppression of the response to the unwanted sideband depends on the accuracy of the quadrature phase relationships, the matching of the frequency responses of the mixers and filters, and the insertion loss of the phase lag network. In practice, for conversion from a few gigahertz to baseband, suppression to a level of −20 dB is routinely achievable. With careful design, suppression to a level approaching −30 dB can be obtained (Archer et al. 1981).

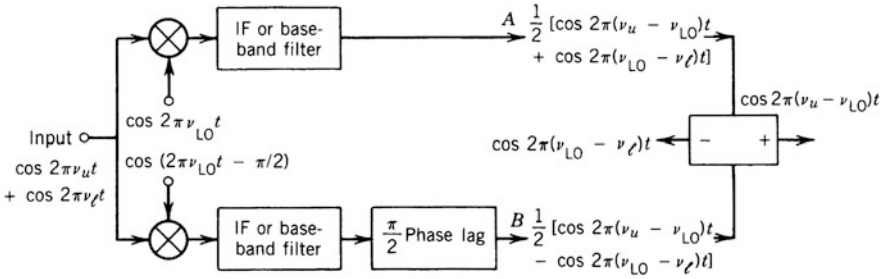

Fig. A7.1 Schematic illustration of the principle of the sideband-separating (image-rejection) mixer. The upper-sideband response is obtained from the sum of the outputs A and B, and the lower-sideband response from the difference of these outputs.

Appendix 7.2 Dispersion in Optical Fiber

For a frequency component, ν_m, of a signal modulated onto an optical carrier, $A\sin(2\pi\nu_{\text{opt}} + \phi)$, and transmitted down a fiber, the resulting signal intensity at the output of the fiber can be represented by

$$\begin{aligned} &A^2[1 + m\cos(2\pi\nu_m t)]\sin^2(2\pi\nu_{\text{opt}}t + \phi) \\ &\quad = A^2\sin^2(2\pi\nu_{\text{opt}}t + \phi) \\ &\qquad + \frac{A^2 m}{2}\sin[2\pi(\nu_{\text{opt}} + \nu_m)(t - \Delta t) + \phi]\sin(2\pi\nu_{\text{opt}}t + \phi) \\ &\qquad + \frac{A^2 m}{2}\sin[2\pi(\nu_{\text{opt}} - \nu_m)(t + \Delta t) + \phi]\sin(2\pi\nu_{\text{opt}}t + \phi)\ , \end{aligned} \tag{A7.1}$$

where m is the modulation index. This equation resembles the usual representation for amplitude modulation in communications, except that here, the carrier *power* varies linearly with the modulation. Thus, on the left side, the square of the carrier expression is used. For the terms of frequency $\nu_{\text{opt}} \pm \nu_m$, the time has been offset by $\pm\Delta t$ to represent the effects of the variation of propagation velocity with frequency. Δt can take both positive and negative values depending on the sign of the dispersion $\mathcal{D}$ shown in Fig. 7.3. Each term in Eq. (A7.1) is proportional to optical power and, thus, also to the modulation amplitude. By applying the identity for the product of two sines to each term on the right side of Eq. (A7.1), and ignoring DC and optical frequency terms, we obtain for the amplitude at the output of the optical receiver,

$$\begin{aligned} &\frac{A^2 m}{4}\left\{\cos[2\pi\nu_m(t + \Delta t) - 2\pi\nu_{\text{opt}}\Delta t] + \cos[2\pi\nu_m(t - \Delta t) - 2\pi\nu_{\text{opt}}\Delta t]\right\} \\ &\qquad = \frac{A^2 m}{2}\left\{\cos[2\pi(\nu_m t - \nu_{\text{opt}}\Delta t)]\cos(2\pi\nu_m\Delta t)\right\}\ . \end{aligned} \tag{A7.2}$$

The free-space wavelength corresponding to frequency ν_{opt} is λ_{opt}, and the wavelength difference between frequencies ν_{opt} and $\nu_{\text{opt}} + \nu_m$ is $\lambda_{\text{opt}}^2\nu_m/c$ (since $\nu_{\text{m}} \ll \nu_{\text{opt}}$). If $\mathcal{D}$ is the dispersion and ℓ is the length of the fiber, $\Delta t = \mathcal{D}\ell\lambda_{\text{opt}}^2\nu_m/c$, and $\nu_{\text{opt}}\Delta t = \mathcal{D}\ell\lambda_{\text{opt}}\nu_m$. Thus, the recovered modulation can be written as

$$\frac{A^2 m}{2}\left\{\cos[2\pi\nu_m(t - \mathcal{D}\ell\lambda_{\text{opt}})]\cos(2\pi\nu_m^2\mathcal{D}\ell\lambda_{\text{opt}}^2/c)\right\}\ . \tag{A7.3}$$

The phase change induced by Δt at the carrier frequency ν_{opt} appears in the phase of the modulation frequency in the first cosine function in Eq. (A7.2). At frequency ν_m, this phase term is equivalent to a time delay $\mathcal{D}\ell\lambda_{\text{opt}}$, as seen in Eq. (A7.3). This delay is much larger than Δt and represents the difference between the phase and the group velocities in the fiber. The second cosine modifies the amplitude of the modulation

component ν_m. For example, with dispersion $\mathcal{D} = 2$ ps/(km·nm) (note that this is equal to 2×10^{-6}s m^{-2}), $\ell = 50$ km, $\lambda_{\text{opt}} = 1550$ nm, and $\nu_m = 10$ GHz, we obtain $\Delta t = 8$ ps, $\mathcal{D}\ell\lambda_{\text{opt}} = 155$ ns, and the response at frequency ν_m is reduced by 1.1 dB relative to the low-frequency end of the modulation spectrum. Note that we have assumed above that the frequency spread of the laser results entirely from the modulation spectrum, which is justifiable for a high-quality laser with an external modulator. Modulation of a diode laser by varying the voltage across it can result in unwanted frequency modulation, further spreading the optical spectrum.

Appendix 7.3 Alias Sampling

After Nyquist sampling of a signal band $n\Delta\nu$ to $(n+1)\Delta\nu$, where n is an integer, the frequency band of the sampled data is 0 to $\Delta\nu$ and does not depend on the frequency of the band at the sampler input.[10] This effect is known as alias sampling. To illustrate this situation, consider a Fourier component $A\sin(2\pi\nu t + \phi)$, with arbitrary amplitude and phase, within a band 0 to $\Delta\nu$. The band is sampled at the Nyquist rate, the sample times being $t = m/(2\Delta\nu)$ where $m = 0, 1, 2, \ldots$. The sampled values of the component are $A\sin(\phi), A\sin(\frac{\pi\nu}{\Delta\nu} + \phi), A\sin(\frac{2\pi\nu}{\Delta\nu} + \phi), \ldots$. Now consider the case in which the same input band has been converted to the range $\Delta\nu$ to $2\Delta\nu$. The frequency is higher by $\Delta\nu$, so the original component becomes

$$A\sin[2\pi(\nu + \Delta\nu)t + \phi] = A\sin(2\pi\nu t + \phi)\cos(2\pi\Delta\nu t) + A\cos(2\pi\nu t + \phi)\sin(2\pi\Delta\nu t)\,. \tag{A7.4}$$

Again, sampling at times $m/(2\Delta\nu)$, we obtain for the components: $A\sin(\phi)$, $-A\sin(\frac{\pi\nu}{\Delta\nu} + \phi)$, $A\sin(\frac{2\pi\nu}{\Delta\nu} + \phi)$, $\ldots$. The result is the same as before except that the sign is reversed for odd values of m. Further investigation shows that this sign reversal occurs when n has an odd value. Since the sign reversal occurs for both signals of a cross-correlated pair, it has no effect on the product. Thus, for any value of n, the result at the correlator output is the same as for a baseband input to the sampler. Thus, sampling of the band $n\Delta\nu$ to $(n+1)\Delta\nu$ has the effect of converting the band downward by $n\Delta\nu$, sometimes referred to as alias sampling.

[10] This is the case, for example, in both the VLA and ALMA, where a 1 : 2 frequency ratio between the lower and upper edges of the final analog IF response is used because it is easier to maintain uniform gain than with a baseband response.

References

Agrawal, G.P., *Fiber-Optic Communication Systems*, Wiley, New York (1992)

Allen, L.R., and Frater, R.H., Wideband Multiplier Correlator, *Proc. IEEE*, **117**, 1603–1608 (1970)

Archer, J.W., Caloccia, E.M., and Serna, R., An Evaluation of the Performance of the VLA Circular Waveguide System, *IEEE Trans. Microwave Theory Tech.*, **MTT-28**, 786–791 (1980)

Archer, J.W., Granlund, J., and Mauzy, R.E., A Broadband UHF Mixer Exhibiting High Image Rejection Over a Multidecade Baseband Frequency Range, *IEEE J. Solid-State Circuits*, **SC-16**, 385–392 (1981)

Baars, J.W.M., van der Brugge, J.F., Casse, J.L., Hamaker, J.P., Sondaar, L.H., Visser, J.J., and Wellington, K.J., The Synthesis Radio Telescope at Westerbork, *Proc. IEEE*, **61**, 1258–1266 (1973)

Bagri, D.S., and Thompson, A.R., Hardware Considerations for High Dynamic Range Imaging, *Radio Interferometry: Theory, Techniques and Applications*, IAU Colloq. 131, T. J. Cornwell and R. A. Perley, Eds., Astron. Soc. Pacific Conf. Ser., **19**, 47–54 (1991)

Batty, M.J., Jauncey, D.L., Rayner, P.T., and Gulkis, S., Tidbinbilla Two-Element Interferometer, *Astron. J.*, **87**, 938–944 (1982)

Beauchamp, K.G., *Walsh Functions and Their Applications*, Academic Press, London (1975)

Borella, M.S., Jue, J.P., Banergee, D., Ramamurthy, B., and Mukherjee, B., Optical Components for WDM Lightwave Networks, *Proc. IEEE*, **85**, 1274–1307 (1997)

Bracewell, R.N., Colvin, R.S., D'Addario, L.R., Grebenkemper, C.J., Price, K.M., and Thompson, A.R., The Stanford Five-Element Radio Telescope, *Proc. IEEE*, **61**, 1249–1257 (1973)

Callen, H.B., and Welton, T.A., Irreversibility and Generalized Noise, *Phys. Rev.*, **83**, 34–40 (1951)

Carlson, B.R., and Dewdney, P.E., Efficient Wideband Digital Correlation, *Electronics Lett.*, **36**, 987–988 (2000)

Casse, J.L., Woestenburg, E.E.M., and Visser, J.J., Multifrequency Cryogenically Cooled Front-End Receivers for the Westerbork Synthesis Radio Telescope, *IEEE Trans. Microwave Theory Tech.*, **MTT-30**, 201–209 (1982)

Coe, J.R., Interferometer Electronics, *Proc. IEEE*, **61**, 1335–1339 (1973)

D'Addario, L.R., Orthogonal Functions for Phase Switching and a Correction to ALMA Memo 287, ALMA Memo 385, National Radio Astronomy Observatory (2001)

D'Addario, L.R., Passband Shape Deviation Limits, ALMA Memo 452, National Radio Astronomy Observatory (2003)

Davies, J.G., Anderson, B., and Morison, I., The Jodrell Bank Radio-Linked Interferometer Network, *Nature*, **288**, 64–66 (1980)

de Vos, M., Gunst, A.W., and Nijboer, R., The LOFAR Telescope: System Architecture and Signal Processing, *Proc. IEEE*, **97**, 1431–1437 (2009)

Elsmore, B., Kenderdine, S., and Ryle, M., Operation of the Cambridge One-Mile Diameter Radio Telescope, *Mon. Not. R. Astron. Soc.*, **134**, 87–95 (1966)

Emerson, D.T., *The Optimum Choice of Walsh Functions to Minimize Drift and Cross-Talk*, Working Report 127, IRAM, Grenoble, July 18 (1983)

Emerson, D.T., Walsh Function Demodulation in the Presence of Timing Errors, Leading to Signal Loss and Crosstalk, ALMA Memo 537, National Radio Astronomy Observatory (2005)

Emerson, D.T., Walsh Function Definition for ALMA, ALMA Memo 565, National Radio Astronomy Observatory (2007)

Emerson, D.T., Walsh Function Choices for 64 Antennas, ALMA Memo 586, National Radio Astronomy Observatory (2009)

Erickson, W.C., Mahoney, M.J., and Erb, K., The Clark Lake Teepee-Tee Telescope, *Astrophys. J. Suppl.*, **50**, 403–420 (1982)

Fowle, F.F., The Transposition of Electrical Conductors, *Trans. Am. Inst. Elect. Eng.*, **23**, 659–689 (1904)

Gardner, F.M., *Phaselock Techniques*, 2nd ed., Wiley, New York (1979)

Granlund, J., Thompson, A.R., and Clark, B.G., An Application of Walsh Functions in Radio Astronomy Instrumentation, *IEEE Trans. Electromag. Compat.*, **EMC-20**, 451–453 (1978)

Harmuth, H.F., Applications of Walsh Functions in Communications, *IEEE Spectrum*, **6(11)**, 82–91 (1969)

Harmuth, H.F., *Transmission of Information by Orthogonal Functions*, 2nd ed., Springer-Verlag, Berlin (1972)

Kerr, A.R., Suggestions for Revised Definitions of Noise Quantities, Including Quantum Effects, *IEEE Trans. Microwave Theory Tech.*, **47**, 325–329 (1999)

Kerr, A.R., Feldman, M.J., and Pan, S.-K., Receiver Noise Temperature, the Quantum Noise Limit, and the Role of Zero-Point Fluctuations, *Proc. 8th Int. Symp. Space Terahertz Technology* (1997), pp. 101–111; also available as MMA Memo 161, National Radio Astronomy Observatory (1997)

Keto, E., Three-Phase Switching with m-Sequences for Sideband Separation in Radio Interferometry, *Publ. Astron. Soc. Pacific*, **112**, 711–715 (2000)

Kraus, J.D., *Radio Astronomy*, 2nd ed., Cygnus-Quasar Books, Powell, OH (1986)

Little, A.G., A Phase-Measuring Scheme for a Large Radiotelescope, *IEEE Trans. Antennas Propag.*, **AP-17**, 547–550 (1969)

Moran, J.M., The Submillimeter Array, in *Advanced Technology MMW, Radio, and Terahertz Telescopes*, Phillips, T.G., Ed., Proc. SPIE, **3357**, 208–219 (1998)

Napier, P.J., Bagri, D.S., Clark, B.G., Rogers, A.E.E., Romney, J.D., Thompson, A.R., and Walker, R.C., The Very Long Baseline Array, *Proc. IEEE*, **82**, 658–672 (1994)

Napier, P.J., Thompson, A.R., and Ekers, R.D., The Very Large Array: Design and Performance of a Modern Synthesis Radio Telescope, *Proc. IEEE*, **71**, 1295–1320 (1983)

National Radio Astronomy Observatory, *A Proposal for a Very Large Array Radio Telescope*, Vol. II, National Radio Astronomy Observatory, Green Bank, WV (1967), ch. 14

Nyquist, H., Thermal Agitation of Electric Charge in Conductors, *Phys. Rev.*, **32**, 110–113 (1928)

Padin, S., A Wideband Analog Continuum Correlator for Radio Astronomy, *IEEE Trans. Instrum. Meas.*, **IM-43**, 782–784 (1994)

Paley, R.E.A.C., A Remarkable Set of Orthogonal Functions, *Proc. London Math. Soc.*, **34**, 241–279 (1932)

Payne, J.M., Millimeter and Submillimeter Wavelength Radio Astronomy, *Proc. IEEE*, **77**, 993–1071 (1989)

Payne, J.M., D'Addario, L., Emerson, D.T., Kerr, A.R., and Shillue, B., Photonic Local Oscillator for the Millimeter Array, in *Advanced Technology MMW, Radio, and Terahertz Telescopes*, Phillips, T.G., Ed., Proc. SPIE, **3357**, 143–151 (1998)

Payne, J.M., Lamb, J.W., Cochran, J.G., and Bailey, N.J., A New Generation of SIS Receivers for Millimeter-Wave Radio Astronomy, *Proc. IEEE*, **82**, 811–823 (1994)

Perley, R., Napier, P., Jackson, J., Butler, B., Carlson, B., Fort, D., Dewdney, P., Clark, B., Hayward, R., Durand, S., Revnell, M., and McKinnon, M., The Expanded Very Large Array, *Proc. IEEE*, **97**, 1448–1462 (2009)

Phillips, T.G., Millimeter and Submillimeterwave Receivers, in *Astronomy with Millimeter and Submillimeter Wave Interferometry*, Ishiguro, M., and Welch, W.J., Eds., Astron. Soc. Pacific Conf. Ser., **59**, 68–77 (1994)

Phillips, T.G., and Woody, D.P., Millimeter- and Submillimeter-Wave Receivers, *Ann. Rev. Astron. Astrophys.*, **20**, 285–321 (1982)

Pospieszalski, M.W., Extremely Low-Noise Amplification with Cryogenic FET's and HFET's: 1970–2004, *Microw. Mag.*, **6**, 62–75 (2005)

Prabu, T., Srivani, K.S., Roshi, D.A., Kamini, P.A., Madhavi, S., Emrich, D., Crosse, B., Williams, A.J., Waterson, M., Deshpande, A.A., and 48 coauthors, A Digital Receiver for the Murchison Widefield Array, *Experimental Astron.*, **39**, 73–93 (2015)

Read, R.B., Two-Element Interferometer for Accurate Position Determinations at 960 Mc, *IRE Trans. Antennas Propag.*, **AP-9**, 31–35 (1961)

Reid, M.S., Clauss, R.C., Bathker, D.A., and Stelzried, C.T., Low Noise Microwave Receiving Systems in a Worldwide Network of Large Antennas, *Proc. IEEE*, **61**, 1330–1335 (1973)

Sinclair, M.W., Graves, G.R., Gough, R.G., and Moorey, G.G., The Receiver System, *J. Elect. Electronics Eng. Aust.*, **12**, 147–160 (1992)

Swarup, G., and Yang, K.S., Phase Adjustment of Large Antennas, *IEEE Trans. Antennas Propag.*, **AP-9**, 75–81 (1961)

Thompson, A.R., *Tolerances on Polarization Mismatch*, VLB Array Memo 346, National Radio Astronomy Observatory (1984)

Thompson, A.R., Clark, B.G., Wade, C.M., and Napier, P.J., The Very Large Array, *Astrophys. J. Suppl.*, **44**, 151–167 (1980)

Thompson, A.R., and D'Addario, L.R., Frequency Response of a Synthesis Array: Performance Limitations and Design Tolerances, *Radio Sci.*, **17**, 357–369 (1982)

Thompson, A.R., and D'Addario, L.R., Relative Sensitivity of Double- and Single- Sideband Systems for Both Total Power and Interferometry, ALMA Memo 304, National Radio Astronomy Observatory (2000)

Thompson, M.C., Wood, L.E., Smith, D., and Grant, W.B., Phase Stabilization of Widely Separated Oscillators, *IEEE Trans. Antennas Propag.*, **AP-16**, 683–688 (1968)

Tiuri, M.E., and Räisänen, A.V., Radio-Telescope Receivers, in *Radio Astronomy*, 2nd ed., J. D. Kraus, Cygnus-Quasar Books, Powell, OH (1986), ch. 7

Tucker, J.R., Quantum Limited Detection in Tunnel Junction Mixers, *IEEE J. Quantum Elect.*, **QE-15**, 1234–1258 (1979)

Tucker, J.R., and Feldman, M.J., Quantum Detection at Millimeter Wavelengths, *Rev. Mod. Phys.*, **57**, 1055–1113 (1985)

Valley, S.L., Ed., *Handbook of Geophysics and Space Environments*, Air Force Cambridge Research Laboratories, Bedford, MA (1965), pp. 3-20–3-22

Walsh, J.L., A Closed Set of Orthogonal Functions, *Ann. J. Math.*, **55**, 5–24 (1923)

Webber, J.C., and Pospieszalski, M.W., Microwave Instrumentation for Radio Astronomy, *IEEE Trans. Microwave Theory Tech.*, **MTT-50**, 986–995 (2002)

Weinreb, S., Balister, M., Maas, S., and Napier, P.J., Multiband Low-Noise Receivers for a Very Large Array, *IEEE Trans. Microwave Theory Tech.*, **MTT-25**, 243–248 (1977a)

Weinreb, S., Fenstermacher, D.L., and Harris, R.W., Ultra-Low-Noise 1.2- to 1.7-GHz Cooled GaSaFET Amplifiers, *IEEE Trans. Microwave Theory Tech.*, **MTT-30**, 849–853 (1982)

Weinreb, S., Predmore, R., Ogai, M., and A. Parrish, Waveguide System for a Very Large Antenna Array, *Microwave J.*, **20**, 49–52 (1977b)

Welch, W.J., Forster, J.R., Dreher, J., Hoffman, W., Thornton, D.D., and Wright, M.C.H., An Interferometer for Millimeter Wavelengths, *Astron. Astrophys.*, **59**, 379–385 (1977)

Welch, W.J., Thornton, D.D., Plambeck, R.L., Wright, M.C.H., Lugten, J., Urry, L., Fleming, M., Hoffman, W., Hudson, J., Lum, W.T., and 27 coauthors, The Berkeley–Illinois–Maryland–Association Millimeter Array, *Publ. Astron. Soc. Pacific*, **108**, 93–103 (1996)

Wengler, M.J., and Woody, D.P., Quantum Noise in Heterodyne Detection, *IEEE J. Quantum Electr.*, **QE-23**, 613–622 (1987)

Wootten, A., Atacama Large Millimeter Array (ALMA), in *Large Ground-Based Telescopes*, Oschmann, J.M., and Stepp, L.M., Eds., Proc. SPIE, **4837**, 110–118 (2003)

Wootten, A., and Thompson, A.R., The Atacama Large Millimeter/Submillimeter Array, *Proc. IEEE*, **97**, 1463–1471 (2009)

Wright, M.C.H., Clark, B.G., Moore, C.H., and Coe, J., Hydrogen-Line Aperture Synthesis at the National Radio Astronomy Observatory: Techniques and Data Reduction, *Radio Sci.*, **8**, 763–773 (1973)

Young, A.C., McCulloch, M.G., Ables, S.T., Anderson, M.J., and Percival, T.M., The Local Oscillator System, *Proc. IREE Aust.*, **12**, 161–172 (1992)

Zorin, A.B., Quantum Noise in SIS Mixers, *IEEE Trans. Magn.*, **MAG-21**, 939–942 (1985)